Hydride Mobility in Trinuclear Sulfido Clusters with the Core $[Rh_3(\mu\text{-}H)(\mu_3\text{-}S)_2]$: Molecular Models for Hydrogen Migration on Metal Sulfide Hydrotreating Catalysts

M. Victoria Jiménez, Fernando J. Lahoz, Lenka Lukešová, José R. Miranda, Francisco J. Modrego, Duc H. Nguyen, Luis A. Oro* and Jesús J. Pérez-Torrente* [a]

[a] Dr. M. V. Jiménez, Dr. F. J. Lahoz, L. Lukešová, J. R. Miranda, Dr. F. J. Modrego, Dr. D. H. Nguyen, Prof. Dr. L. A. Oro, Prof. Dr. J. J. Pérez-Torrente

Departamento de Química Inorgánica, Instituto Universitario de Catálisis Homogénea, Instituto de Ciencia de Materiales de Aragón, Universidad de Zaragoza-C.S.I.C.

50009-Zaragoza (Spain).

Fax: (+34) 976761143

E-mail: oro@unizar.es, perez@unizar.es

Supporting information for this article is available on the WWW under http://dx.doi.org/10.1002/chem.2010xxxxx.

Abstract

Reaction of $[Rh(\mu\text{-}SH)\{P(OPh)_3\}_2]_2$ with complexes $[\{M(\mu\text{-}Cl)(diolef)\}_2]$ in the presence of NEt_3 affords the hydrido-sulfido clusters $[Rh_3(\mu\text{-}H)(\mu_3\text{-}S)_2\{P(OPh)_3\}_4(diolef)]$ (diolef = cod, **1**; nbd, **2**; tfb, **3**) and $[Rh_2Ir(\mu\text{-}H)(\mu_3\text{-}S)_2\{P(OPh)_3\}_4(cod)]$ (**4**). Cluster **1** can be also obtained by reaction of $[Rh(\mu\text{-}SH)\{P(OPh)_3\}_2]_2$ with $[Rh(\mu\text{-}OMe)(cod)]_2$ although the main product of the reaction with $[Ir(\mu\text{-}OMe)(cod)]_2$ was the cluster $[RhIr_2(\mu\text{-}H)(\mu_3\text{-}S)_2\{P(OPh)_3\}_2(cod)_2]$ (**5**). The molecular structures of clusters **1** and **4** have been determined by X-ray diffraction methods. The deprotonation of a hydrosulfido ligand in compound $[Rh(\mu\text{-}SH)(CO)(PPh_3)]_2$ by mononuclear acetylacetonato [M(acac)(diolef)] complexes results in the formation of hydrido-sulfido clusters $[Rh_3(\mu\text{-}H)(\mu_3\text{-}S)_2(CO)_2(PPh_3)_2(diolef)]$ (diolef = cod, **6**; nbd, **7**) and $[Rh_2Ir(\mu\text{-}H)(\mu_3\text{-}S)_2(CO)_2(PPh_3)_2(cod)]$ (**8**). Clusters **1**-**3** and **5** exist in solution as two interconverting isomers having the bridging hydride ligand at different edges. The energy barriers for the hydride exchange determined by ^1H 2D-EXSY NMR spectroscopy are in the range 67-72 kJ mol^{-1}. DFT calculations on the model compound $[Rh_3(\mu\text{-}H)(\mu_3\text{-}S)_2(PH_3)_4(cod)]$ have established that the hydride migration around the bipiramidal-trigonal $[Rh_3S_2]$ core involves a μ_3-sulfido bridging ligand through the hydrosulfido-sulfido intermediate $[Rh_3(\mu_3\text{-}SH)(\mu_3\text{-}S)(PH_3)_4(cod)]$ with energy barriers comparable to those observed experimentally. Cluster **8** exists as three isomers that arise from the disposition of the PPh_3 ligands in the cluster (*cis* and *trans*) and the location of the hydride ligand. Two-dimensional exchange spectroscopy substantiates a static bridging hydride ligand in *trans*-**8b** and the existence of the equilibrium *trans*-**8a** ⇆ *cis*-**8b** that supports an hydride exchange pathway through a turnstile mechanism with a similar activation energy. The dynamic behaviour of clusters having bulky triphenylphosphite ligands, $[Rh_3(\mu\text{-}H)(\mu_3\text{-}S)_2\{P(OPh)_3\}_4(diolef)]$, that involves the hydrogen migration from rhodium to sulphur with a

switch from hydride to proton character, is significant to understand the hydrogen diffusion on the surface of metal sulfide hydrotreating catalysts.

Introduction

The chemistry of transition metal sulfido clusters has been attracting significant attention with regard to the active sites of metalloenzimes and industrial metal sulfide catalysts for hydrotreating processes, in particular, for hydrodesulfurization (HDS) of fossil fuels.[1-3] The controlled construction of sulfido clusters has been a major objective in this field and the development of rational synthetic methods has allowed the preparation of a wide range of multimetallic sulfido clusters with the desired metal composition and metal-sulfur framework.[4-7]

Hydrosulfido metal complexes have been recognized as fundamental building blocks for the synthesis of polynuclear complexes and clusters.[8] In this context, bis(hydrosulfido) mononuclear complexes, as for example $[Cp_2M(SH)_2]$ (M = Mo, W),[9] $[Cp^*M(SH)_2(PR_3)]$ (M = Rh, Ir)[10] and $[M(SH)_2(diphos)]$ (M = Pd, Pt),[11] behave as metalloligands for the synthesis of both hydrosulfido- and sulfido-bridged multinuclear complexes.[12] We have reported the application of mononuclear bis(hydrosulfido) titanium and zirconium complexes, $[Cp_2Ti(SH)_2]$ and $[Cp^{tt}{}_2Zr(SH)_2]$ (Cp^{tt} = η^5-1,3-di-*tert*-butylcyclopentadienyl), for the synthesis of *early-late* heterobimetallic complexes (ELHB). The deprotonation of these complexes with mono- and dinuclear d^8 rhodium and iridium compounds containing basic ligands has led to the preparation of heterotrinuclear, $[TiM_2]$ and $[ZrM_2]$,[13] and heterotetranuclear $[TiM_3]$ (M = Rh, Ir)[14] d^0-d^8 sulfido-bridged complexes with incomplete cubane structures, and some unexpected $[Ti_2Rh_4]$ oxosulfido titanium-rhodium clusters with an incomplete doubly-fused cubane structure.[15] Alternative dinuclear precursors for mixed-metal cluster synthesis are the bis(hydrosulfido)-briged complexes $[(Cp^*MCl)_2(\mu_2\text{-}SH)_2]$ (M =

Ru, Rh, Ir) that allowed the synthesis of tri- and pentanuclear heterometallic clusters with $[M'M_2(\mu_3\text{-}S)_2]$ and $[M'M_4(\mu_3\text{-}S)_4]$ cores,[16] and cubano-type homometallic clusters $[M_4(\mu_3\text{-}S)_4]$[17] through condensation processes involving HCl elimination.

We have recently reported the synthesis of bis(hydrosulfido)-bridged dinuclear rhodium complexes $[Rh(\mu\text{-}SH)L_2]_2$ from mononuclear rhodium(I) acetylacetonato complexes and $H_2S(g)$ as hydrosulfido ligand source.[18] In contrast with $[Rh(\mu\text{-}SH)\{P(OPh)_3\}_2]_2$, the complexes $[Rh(\mu\text{-}SH)(CO)(PR_3)]_2$ slowly transform in solution into the 48-electron trinuclear hydrido-sulfido clusters $[Rh_3(\mu\text{-}H)(\mu_3\text{-}S)_2(CO)_3(PR_3)_3]$ (R = Cy, Ph) with the release of $H_2S(g)$ in a reversible way. Related precedent in this chemistry are the clusters $[M_3(\mu\text{-}H)(\mu_3\text{-}S)_2(cod)_3]$ that are formed by reaction of complexes $[M(\mu\text{-}Cl)(cod)]_2$ with NaSH,[19] or [M(acac)(cod)] and $[M(\mu\text{-}OMe)(cod)]_2$ (M = Rh, Ir) with $H_2S(g)$.[18] In full agreement with the stability of these trinuclear hydrido-sulfido clusters, the clusters $[Rh_3(\mu\text{-}H)(\mu_3\text{-}S)_2(CO)_3(PR_3)_3]$ have also been obtained from [Rh(acac)(CO)(PR$_3$)] complexes by control of the $H_2S(g)$ concentration in the reaction media.[19] Stimulated by these findings we envisage the potential of these bis(hydrosulfido)-bridged dinuclear rhodium complexes for the controlled synthesis of mixed-metal sulfido clusters through the selective deprotonation of the hydrosulfido ligands. We report herein on the application of this methodology for the synthesis of diverse homo- and heterotrinuclear hydrido-sulfido clusters with the core $[M_3(\mu\text{-}H)(\mu_3\text{-}S)_2]$. Interestingly, some of these clusters exhibit a mobile hydride ligand that migrates between edge-bridging sites. Kinetic data for the hydride migration process have been obtained by two-dimensional NMR spectroscopy. In addition, the mechanism for the mobility of the hydride ligand, which has been investigated by DFT calculations, is relevant to the possible pathways for the hydrogen diffusion on the surface of metal sulfide hydrotreating catalysts.[1d, 22]

Results

Synthesis and characterization of clusters $[Rh_2M(\mu\text{-}H)(\mu_3\text{-}S)_2\{P(OPh)_3\}_4(diolef)]$ (M = Rh, Ir). Reaction of $[Rh(\mu\text{-}SH)\{P(OPh)_3\}_2]_2$ with half equiv. of $[\{Rh(\mu\text{-}Cl)(cod)\}_2]$ in benzene in the presence of an excess of NEt_3 gave a deep red solution of the hydrido-sulfido cluster $[Rh_3(\mu\text{-}H)(\mu_3\text{-}S)_2\{P(OPh)_3\}_4(cod)]$ (**1**). The cluster was isolated in 82% yield as dark red microcrystals by crystallization from dichloromethane/*n*-hexane at 258 K. The formation of the trinuclear sulfido cluster was confirmed by the ESI– mass spectrum that showed the molecular ion at m/z 1772. The ^1H NMR spectrum of **1** in C_6D_6 showed two resonances of high multiplicity in the high field region corresponding to bridging hydride ligands which suggest the presence of two isomers (**1a** and **1b**) arising form the different location of the bridging hydride ligand in the unsymmetrical molecular framework (Scheme 1). Thus, the resonance triplet of quintuplets (tq) at δ = -14.37 ppm, that became a triplet in the $^1H\{^{31}P\}$ NMR spectrum, was assigned to isomer **1a** with the hydride ligand bridging the two rhodium atoms with triphenylphosphite ligands. The resonance double doublet of triplets (ddt) at δ = -13.75 ppm, that became a double doublet in the $^1H\{^{31}P\}$ NMR spectrum, corresponds to isomer **1b** with the hydride ligand bridging rhodium atoms with triphenylphosphite and cod ligands (Figure 1). In addition, the olefin region of the ^1H NMR spectrum showed three resonances for the =CH protons of the cod ligand, one for **1a** and two for **1b** (^1H–^1H COSY evidence) in agreement with the symmetry of both isomers, C_{2v} and C_s, respectively. Outstandingly, both isomers interconvert in solution as was evidenced by the cross-peaks observed in the ^1H–^1H NOESY spectrum, both in the hydride and olefinic regions (Figure 2). The $^{31}P\{^1H\}$ NMR (C_6D_6) of **1** showed a somewhat broad asymmetric doublet centered at δ = 112.7 ppm (J(Rh,P) ≈ 264 Hz) probably as a consequence of the chemical exchange involving the migration of hydride ligand between Rh–Rh edges.

The reaction of $[Rh(\mu\text{-}SH)\{P(OPh)_3\}_2]_2$ with complexes $[\{Rh(\mu\text{-}Cl)(diolef)\}_2]$ (diolef = nbd, tfb) in benzene in the presence of an excess of NEt_3 gave the clusters $[Rh_3(\mu\text{-}H)(\mu_3\text{-}S)_2\{P(OPh)_3\}_4(nbd)]$ (**2**) and $[Rh_3(\mu\text{-}H)(\mu_3\text{-}S)_2\{P(OPh)_3\}_4(tfb)]$ (**3**) which were isolated as orange microcrystalline solids in 70% and 56% yield, respectively. The clusters have been fully characterized by ESI– MS and multinuclear 1D and 2D NMR spectroscopy. In particular, the high field region of the ^1H NMR spectra in CD_2Cl_2 at low temperature showed two resonances with multiplicities tq and ddt which suggested that the hydride ligand in both clusters is dynamic, which was further confirmed in the ^1H–^1H NOESY spectrum. In contrast with **1**, the $^{31}P\{^1H\}$ NMR (C_6D_6) of both clusters features the expected three resonances, which have been unambiguously assigned to both isomers with the help of the 2D ^1H–^{31}P HMBC spectra. For example, the isomer **3a** features a broad doublet at δ = 112.44 ppm for the equivalent phosphite ligands (C_{2v} symmetry) but two distinct resonances at δ = 111.89 (br d) and 112.75 (br d) ppm were observed for **3b** in agreement with the lower symmetry (C_s).

This synthetic methodology is also applicable to the preparation of the heterometallic hydrido-sulfido cluster $[Rh_2Ir(\mu\text{-}H)(\mu_3\text{-}S)_2\{P(OPh)_3\}_4(cod)]$ (**4**) that was isolated as dark red microcrystals in 68% yield. In contrast with clusters **1**-**3**, the hydride ligand in **4** is static and the cluster exists as a single **b**-type isomer with the bridging hydride ligand at the Rh–Ir edge of the metallic triangle (Scheme 1). Accordingly, the hydride ligand in **4** was observed as a broad doublet at δ = -20.09 ppm (J(Rh,H) = 24.3 Hz) in the ^1H NMR spectrum (C_6D_6) and the olefinic =CH protons of the cod ligand as two broad resonances at δ = 4.18 y 3.53 ppm. In addition, the two sets of nonequivalent phosphorus atoms were observed in the $^{31}P\{^1H\}$ NMR spectrum as two doublets of multiplets at δ = 113.01 and 112.84 ppm (J(Rh,P) ≈ 275 Hz), in full agreement with the C_s symmetry of the cluster.

Molecular structures of $[Rh_3(\mu\text{-}H)(\mu_3\text{-}S)_2\{P(OPh)_3\}_4(cod)]$ (1) and $[Rh_2Ir(\mu\text{-}H)(\mu_3\text{-}S)_2\{P(OPh)_3\}_4(cod)]$ (4). From the similarities of the cell parameters of both crystal structures, it could be inferred the feasible similarities of both molecular structures. In fact, both crystal structures exhibit the presence of analogous trinuclear clusters, disordered dichloromethane molecules and a region, close to an inversion center, where additional highly disordered solvent molecules –interpreted as *n*-hexane– were localized (see experimental for more details).

Simplified molecular representations of both trinuclear clusters have been incorporated in Figures 3 and 4; a comparative list of the most relevant bond distances and angles has been collected in Table 1. From these geometrical parameters it becomes clear that both metal complexes are nearly isostructural, with the only relevant differences associated to the location of the bridging calculated hydrides. In the solid state, the trinuclear clusters exhibit an asymmetric triangular metal core stabilized by two triply bridging sulfido ligands situated at both sides of the M_3 planes, connecting two identical '$Rh\{P(OPh)_3\}_2$' moieties and an additional 'M(cod)' unit (M = Rh (**1**), Ir (**4**)). The M-S bond distances are also reflecting the electron density differences of the metals, showing two long distances (range 2.3406(12)-2.3533(10) Å) to the phosphite-bonded rhodium atoms (Rh(1) and Rh(2)), and one shorter bond length to the olefin-coordinated metals, 2.3191(8) Å in **1** and 2.3283(7) Å in **4**. A similar pattern for the Rh-S bond distances has been observed in the closely related cluster, $[Rh_3(\mu\text{-}H)(\mu_3\text{-}S)_2(CO)_3(PCy_3)_3]$, where also two types of bond lengths –all slightly longer in the latter case– has been reported (2.366 and 2.334(2) Å).[18]

The main differences between both cluster molecules involve the presence of a bridging hydride ligand, which has been included in the model from electrostatic potential energy calculations.[21] In both cases the hydride occupies a nearly coplanar position with the plane defined by the three metals but, as inferred from NMR measurements, while in **1** it is located

connecting Rh(1) and Rh(2) centres, it bridges Rh(1) and Ir atoms in **4**; according with this, the corresponding hydrido-bridged M–M separations (Rh(1)–Rh(2) 2.9332(5) and Rh(1)–Ir 2.9480(4) Å) are significantly shorter than the other two intermetallic distances (means 3.0806(4) (**1**) and 3.0570(3) Å (**4**)). This asymmetry in the M_3 triangle has also its influence on the M-S-M bond angles, in the range 77.16–78.18(3)º for the hydrido-bridged metals, and in the range 80.78–82.67(3)º for the only sulfido-bridged metals. The dissimilarity introduced between **1** and **4** by the different bridging hydride location has no evident effect on the rest of the molecular structure and the minor differences observed in the Rh–P (2.1981 *vs.* 2.1880(6) Å, **1** *versus* **4**), in the M–C(cod) (2.175 *vs.* 2.178(2) Å) or in the olefinic C=C bonds (1.389 *vs.* 1.398(5) Å) are in agreement with an isostructural nature for the rest of the molecule.

All these molecular parameters, together with the structural and chemical similarities of both molecules with the closely related cluster $[Rh_3(\mu\text{-}H)(\mu_3\text{-}S)_2(CO)_3(PCy_3)_3]$, bring us to suggest the interpretation of both compounds as 48-valence-electron clusters with two metal-metal bonded 16-electron M^{II} metal centres, with square-pyramidal geometries, and a 16-electron square-planar M^{I} centre, Rh(3) in **1** and Ir in **4**.

Reaction of $[Rh(\mu\text{-}SH)\{P(OPh)_3\}_2]_2$ with $[\{M(\mu\text{-}OMe)(cod)\}_2]$ (M = Rh, Ir). The deprotonation of the hydrosulfido ligands in $[Rh(\mu\text{-}SH)\{P(OPh)_3\}_2]_2$ can be carried out directly by using rhodium or iridium complexes having basic ligands, as for example $[M(\mu\text{-}OMe)(cod)]_2$. In fact, the reaction of $[Rh(\mu\text{-}SH)\{P(OPh)_3\}_2]_2$ with $[Rh(\mu\text{-}OMe)(cod)]_2$ (half equiv.) is an alternative synthesis for cluster $[Rh_3(\mu\text{-}H)(\mu_3\text{-}S)_2\{P(OPh)_3\}_4(cod)]$ (**1**). However, the reaction with $[Ir(\mu\text{-}OMe)(cod)]_2$ is puzzling as it involves the scrambling of d^8-ML_2 metal fragments leading to homo- and heterometallic trinuclear hydrido-sulfido clusters with the cores $[Rh_nIr_{3-n}(\mu\text{-}H)(\mu_3\text{-}S)_2]$ (n = 0, 1, 2 and 3). The monitoring of the reaction by NMR in $[D_8]$-toluene revealed that the full transformation of $[Rh(\mu\text{-}SH)\{P(OPh)_3\}_2]_2$ requires one equiv. of $[Ir(\mu\text{-}OMe)(cod)]_2$. The high field region of the ^1H NMR spectrum (Figure 5)

showed the formation of **4** (14%) along with the clusters $[Rh_3(\mu\text{-}H)(\mu_3\text{-}S)_2\{P(OPh)_3\}_6]$ (12%) and $[Ir_3(\mu\text{-}H)(\mu_3\text{-}S)_2(cod)_6]$[19a] (2%, δ = -21.43 ppm), although the main product of the reaction was the cluster $[RhIr_2(\mu\text{-}H)(\mu_3\text{-}S)_2\{P(OPh)_3\}_2(cod)_2]$ (**5**) (72%). The bridging hydride ligand in $[Rh_3(\mu\text{-}H)(\mu_3\text{-}S)_2\{P(OPh)_3\}_6]$ features a triplet of quintuplets at δ = -14.21 ppm (J(Rh,H) = 29.4 Hz, ^2J(P,H) ≈ 6 Hz) and has been also detected by ESI– MS at m/z = 2234. Cluster **5** has been isolated from the reaction mixture in moderate yield by fractional crystallization as a red-brown microcrystalline solid. The bridging hydride ligand in **5** is dynamic and the cluster exits as two isomers **5a** and **5b** that interconvert in solution as was evidenced in the ^{1}H–^{1}H NOESY spectrum. The hydride ligand in **5a** bridges the two iridium atoms and features a singlet at δ = -21.74 ppm in the ^{1}H NMR (C_6D_6) spectrum whereas that in **5b** the hydride bridges a Rh–Ir edge and consequently, is observed as a broad doublet at δ = -20.09 ppm (J(Rh,H) = 19.5 Hz).

Kinetic study for the hydride exchange in trinuclear hydrido-sulfido clusters by 2D-EXSY spectroscopy. Line-shape analysis and magnetization transfer are the most commonly used techniques for evaluation of reaction rates. However, the 2D EXSY NMR (two dimensional exchange spectroscopy) method has been increasingly applied to the study of complex kinetic processes, fluxional behaviour, rotational barriers and conformational analysis.[22] This technique is also suitable for the study of multisite exchange processes with small chemical shift differences.

The forward and backward chemical exchange rate constants for the equilibrium **a** ⇆ **b** in clusters $[Rh_3(\mu\text{-}H)(\mu_3\text{-}S)_2\{P(OPh)_3\}_4(diolef)]$ (**1** - **3**) and $[RhIr_2(\mu\text{-}H)(\mu_3\text{-}S)_2\{P(OPh)_3\}_2(cod)_2]$ (**5**), k_1 and k_{-1}, have been determined by ^{1}H 2D-EXSY NMR spectroscopy. The essential feature of a quantitative 2D EXSY experiment is the relationship between the intensity of the cross peaks and the rate constants for chemical exchange. For a system involving chemical exchange between two sites it has been shown that the peak amplitude in the 2D-EXSY

spectrum is related to the exchange rate constant, the relaxation rate and the mixing time.[23] The integrals of the exchange cross peaks in the 2D EXSY spectra were processed using the EXSYCalc program to compute the chemical exchange rate constants k_1 and k_{-1}.[24] The activation energies for the forward ($\Delta G_1^{\#}$) and backward ($\Delta G_{-1}^{\#}$) processes were calculated from the Eyring equation.

$$\Delta G^{\#} = - RT \ln(hk/k_B T)$$

The kinetic parameters for the equilibrium **a** ⇆ **b** are summarized in Table 2. The rate constants at room temperature were calculated to be 2–10 s^{-1} and the calculated activation barriers are in the narrow range of 67–72 kJ mol^{-1}. On the other hand, the calculated equilibrium constants K obtained from the determined rate constants (k_1/ k_{-1}) are in agreement with the experimental values obtained from the same sample by integration of the both hydride resonances in an experiment recorded with the same relaxation time.

The derived rate constants and energy barriers for the rhodium clusters **1**–**3** are very similar which suggest a little influence of the steric and electronic properties of the diolefin ancillary ligand on the Rh(diolef) metal fragment, that is bonded to the hydride ligand in the **b**-type isomer. In addition, the similarities of these values with those measured for compound **5** also points out that the metal composition of the trimetallic core has only a weak influence upon the hydride migration. The largest difference between $\Delta G_1^{\#}$ and $\Delta G_{-1}^{\#}$ was found in cluster **5** and thus, the migration of the hydride ligand from the Rh–Ir edge to the Ir–Ir has an energy barrier 1.9 kJ mol^{-1} lower than the reverse process which is consistent with a weaker Rh–H bond..

The energy barrier for the migration of the hydride ligand in cluster **1** has been also determined by a variable temperature ^{1}H NMR study in [D_8]-toluene. Thus, the hydride resonances at δ = -12.34 and -13.00 ppm coalesce at approximately 373 K to give a broad average resonance at δ = -12.79 ppm. The calculated $\Delta G^{\neq}_c$ value using the Gutowsky-Holm[25]

and the Eyring equations is about 73 kJ mol^{-1} and compares well with the value determined by 2D-EXSY NMR spectroscopy at 300 K.

The energy barriers found in trinuclear hydrido-sulfido clusters are well in the range of those calculated in related trinuclear clusters. Previous studies have shown that the measured activation barriers for hydride migration range from 13 kJ mol^{-1} to greater than 80 kJ mol^{-1}.[26] It has been assumed that hydride fluxionality occurs through changes in the coordination mode of the hydride ligand between doubly bridging and either terminal or triply bridging. However, the mechanism and rate behaviour are still poorly understood because of the hydride migration is complicated by the possible motion of other ligands.

Mechanism for the hydride mobility in trinuclear hydrido-sulfido clusters. Hydride mobility is a common feature of metal clusters chemistry. The migration of hydride ligands in trimetallic clusters has been observed in several cases although, in the spite of several mechanistic proposals,[19, 27-30] the mechanisms have not been fully characterized. Hydride migration between edge-bridging positions is believed to occur through terminal hydride intermediates by a turnstile mechanism. However, the hydride migration process can be assisted by other ligands in the cluster as was demonstrated by Morokuma *et al*. for related monocapped triangular $[M_3(CO)_9(\mu\text{-}H)_3(\mu_3\text{-}CH)]$ (M = Ru, Os) complexes.[31] They propose the movement of the hydride ligand from a bridging edge of the trinuclear framework to the capping methylidine ligand and then, the migration of the former methylidine hydrogen atom from the capping ligand to the adjacent edge of the metallic framework. This process occurs via a terminal hydride ligand and also involves a turnstile movement of the "$Ru(CO)_3H$" fragment. In addition, hydride fluxionality has also been observed in complexes where either the size of the ligands or their chelating role, such as dppm,[27] prevents a turnstile-like mechanism.

The size of the phosphite ligands in cluster $[Rh_3(\mu\text{-}H)(\mu_3\text{-}S)_2\{P(OPh)_3\}_4(cod)]$ (**1**) makes a turnstile-like mechanism quite difficult as it requires: i) the movement of the hydride ligand from bridging to a terminal position, ii) the concerted rotation of both phosphite and hydride ligands, and iii) the migration of hydride ligand towards the adjacent edge of the trimetallic planar core. We have studied the direct transfer form the metal-metal edge to the sulfido ligand as an alternative pathway to explain the fluxional movement of the hydride ligand. In fact, the lone pair on the μ_3-S ligands is able to support protonation in a transient intermediate between the alternative M–M bridging positions. The movement of the hydride ligand as a proton keeps the electron count of the $[M_3S_2]$ core constant without requiring any extensive structural or connectivity changes. Clusters having triply-bridging hydrosulfido ligands, μ_3-SH, are scarce and only a handful cubane clusters, $[\{PtMe_3\}_4(\mu_3\text{-}SH)_4]$ and $[\{M(CO)_3\}_4(\mu_3\text{-}SH)_4]$ (M = Mn, Re),[32] and trinuclear complexes having the core $[M_3(\mu_3\text{-}SH)_2]$ (M = Cu, Ag)[33] have been described. In contrast, the triple bridge coordination mode of thiolato ligands, μ_3-SR, has been found in transition metal clusters and rhodium trinuclear aggregates.[34]

This mechanism via a μ_3-SH intermediate (Figure 6) has been analyzed by DFT calculations. The compound **1** has been modeled as $[Rh_3(\mu\text{-}H)(\mu_3\text{-}S)_2(PH_3)_4(cod)]$ (**1'**) without symmetry restrictions. DFT calculations have been performed using the B3LYP functional and 6-31G** basis set for the non-metal atoms. For Rh the LANL2DZ pseudopotential and its associated basis set were used. In the following analysis of structure geometries Rh_P represents the rhodium atoms bonded to phosphine ligands, while Rh_{cod} is the rhodium atom bonded to the cyclooctadiene ligand.

We have found that the two different Rh-Rh hydride bridged isomers (**1a'** and **1b'**) are close in energy, the free energy of the isomer Rh_P–(μ-H)–Rh_{cod} (**1b'**) is +15.4 kJ/mol relative to isomer Rh_P–(μ-H)–Rh_P (**1a'**). The hydride ligand in both isomers bridges two rhodium atoms

and lies in the Rh_3 plane. Movement of the hydride ligand between both isomers occurs via a trinuclear hydrosulfido-sulfido intermediate [$Rh_3(\mu_3$-SH)(μ_3-S)($PH_3)_4$(cod)] (**1c'**), which has a free energy of +50.2 kJ/mol relative to the Rh_P–(μ-H)–Rh_P isomer (**1a'**).

The most stable isomer of [$Rh_3(\mu$-H)(μ_3-$S)_2(PH_3)_4$(cod)] at this level of calculation is the symmetric species **1a'** where the hydride bridged Rh_P–Rh_P separation is 2.88 Å (exp. 2.932(5)Å). The Rh_P–P distances are all close and they have a value of 2.4 Å. The bridging hydride ligand is located in a symmetric position at a distance of 1.75 Å of both rhodium atoms. The μ_3-S ligand is located at 2.42 Å of the Rh_P atoms (*ca.* 2.35 Å. exp) and at 2.39 Å of the Rh_{cod} atom (*ca.* 2.32 Å, exp.).

The isomer **1b'** has the hydride ligand bridging the Rh_P–Rh_{cod} atoms. At this level of calculations its free energy is +15.4 kJ/mole relative to its most stable counterpart. Both non-bridged edges have similar length and the bridged Rh_p–Rh_{cod} distance is the shorter metal-metal separation at 2.91 Å. The non-bridged Rh_P–Rh_{cod} pair is considerably longer than the bridged one, 3.29 Å. The formerly bridged Rh_P–Rh_P distance increases to a value of 3.24 Å. The hydride ligand in **1b'** sits in an asymmetric position at 1.66 Å from Rh_P and 1.89 from Rh_{cod}. The rhodium phosphine distances for the non-bridged rhodium atom are 2.18 Å whereas the bridged one has a 2.31 Å distance to the PH_3 ligands. The Rh–S distances are all very similar with values between 2.39 and 2.41 Å.

A third isomer of [$Rh_3(\mu$-H)(μ_3-$S)_2(PH_3)_4$(cod)] is [$Rh_3(\mu_3$-SH)(μ_3-S)($PH_3)_4$(cod)] (**1c'**) which appears as a possible intermediate in the hydride movement between the edge bridging positions. It has a free energy of +50.2 kJ/mole above the most stable isomer. All the rhodium atoms are non-bridged and the three Rh–Rh distances are similar, around 3.34 Å. The Rh_P–P distances trans to the μ_3-SH ligands are 2.24 Å and those *trans* to μ_3-S only slightly longer, 2.27 Å. The μ_3-SH group is located at 2.40 Å from Rh_P and 2.43 from Rh_{cod} while the μ_3-S ligand is at *ca.* 2.44 Å from all three Rh atoms.

The transition states that interconvert all the three isomers, **TS_a** and **TS_b**, have been located and characterized by vibrational analysis. A visual inspection of the imaginary frequency in each case shows the relationship between the transition states and the isomers that they connect. The activation energy from the Rh_p–(μ-H)–Rh_p isomer (**1a'**) to **TS_a** leading to the intermediate [Rh_3(μ$_3$-SH)(μ$_3$-S)(PH_3)$_4$(cod)] (**1c'**) is 75.1 kJ/mol, whereas from **1c'** to the Rh_p–(μ-H)–Rh_{cod} isomer (**1b'**) the corresponding transition state, **TS_b**, is located +82.4 kJ/mol above the most stable species and 32.2 kJ/mole relative to **1c'**.

In **TS_a**, the transition state from Rh_p–(μ-H)–Rh_p (**1a'**) to [Rh_3(μ$_3$-SH)(μ$_3$-S)(PH_3)$_4$(cod)] (**1c'**), the hydrogen atom has lost most of its hydridic character and, in fact, the S-H distance of 1.36 Å is very close to the eventual S–H distance of 1.35 Å in the final intermediate. Accordingly the Rh_P–H distances are very long and have a value of 2.74 Å in the transition state while in the bridged starting isomer they were 1.75 Å (see above). In addition, the Rh_p–Rh_p distance has elongated from 2.88 to 3.12 Å.

The second transition state, **TS_b**, relates Rh_P-(μ-H)-Rh_{cod} (**1b'**) and [Rh_3(μ$_3$-SH)(μ$_3$-S)(PH_3)$_4$(cod)] (**1c'**). The S-H distance of 1.36 Å is again very close to the final distance in the intermediate. The Rh_P-Rh_{cod} distances elongates to 3.33 Å in the transition state, from 2.91 Å and finish at 3.35 Å in the intermediate **1c'**. The hydride-rhodium distances increases from 1.42 to 2.53 Å (Rh_P-H) and from 1.89 to 2.90 Å (Rh_{cod}-H). On the other hand, the Rh_P-P distance at the bridged rhodium shortens slightly and gradually as the hydrogen atom is transferred to its eventual SH position. It starts at 2.31 Å and then to 2.29 Å in the transition state and eventually to 2.27 Å in the intermediate **1c'**.

Synthesis and characterization of clusters [Rh_2M(μ-H)(μ$_3$-S)$_2$(CO)$_2$(PPh_3)$_2$(diolef)] (M = Rh, Ir). In sharp contrast with [Rh(μ-SH){P(OPh)$_3$}$_2$]$_2$, the hydrosulfido ligands in [Rh(μ-SH)(CO)(PPh_3)]$_2$ can be also deprotonated by using mononuclear acetylacetonato [M(acac)(diolef)] complexes. Thus, the reaction with [Rh(acac)(cod)] in dichloromethane

gave a brown solution from which the hydrido-sulfido cluster $[Rh_3(\mu\text{-}H)(\mu_3\text{-}S)_2(CO)_2(PPh_3)_2(cod)]$ (**6**) was isolated as a garnet microcrystalline solid in 72% yield. The ^1H NMR spectrum (C_6D_6) features a triplet of triplets at δ = -13.87 ppm (J(Rh,H) = 31.5 and ^2J(P,H) = 5.4 Hz) that suggests a static bridging hydride ligand located at the edge defined by the two Rh(CO)(PPh_3) metal fragments (Scheme 2). The $^{31}P\{^1H\}$ NMR spectrum shows a slightly broad doublet at δ = 34.15 ppm (J(Rh,P) = 152 Hz) for the equivalent triphenylphosphine ligands in the cluster. The shape of this doublet, slightly broad at the base due to small ^2J(Rh,P) and ^3J(P,P) couplings,[13c] suggests a *trans* disposition of both ligands in the cluster resulting in C_2 symmetry.

The clusters $[Rh_3(\mu\text{-}H)(\mu_3\text{-}S)_2(CO)_2(PPh_3)_2(nbd)]$ (**7**) and $[Rh_2Ir(\mu\text{-}H)(\mu_3\text{-}S)_2(CO)_2(PPh_3)_2(cod)]$ (**8**) were prepared using the same synthetic methodology and isolated as garnet microcrystalline solids in good yield. The spectroscopic data suggest that clusters **6** and **7** are isostructural. In particular, the resonance at δ = -13.74 ppm (tt, J(Rh,H) = 32.4 and J(P,H) = 4.2 Hz) in the ^1H NMR spectrum (C_6D_6) of **7** confirms both the static character of the hydride ligand and their location in the cluster (Scheme 2). In contrast, the ^1H NMR spectrum of **8** (C_6D_6) features three resonances in the high field region (Figure 7) that correspond to different isomers derived from the two possible dispositions of the triphenylphosphine ligands in the cluster (*cis* and *trans*) in combination with a mobile bridging hydride ligand (Scheme 3). The observed splitting of the hydride resonance for the two main species at δ = -20.07 and -20.54 ppm (J(Rh,H) ≈ 23 Hz) suggests that the hydride ligand bridges a Rh–Ir edge in the metallic triangle and correspond to the *cis*-**8b** (22 %) and *trans*-**8b** (68 %) isomers, respectively. In the $^{31}P\{^1H\}$ NMR, the *trans*-**8b** isomer displays two doublets of doublets for the no equivalent triphenylphosphine ligands with a ^3J(P,P) = 13 Hz in agreement with their mutual *trans* disposition. In contrast, the *cis*-**8b** isomers features two broad doublets as expected for a much smaller ^3J(P,P) coupling constant. The remaining

hydride resonance exhibits a triplet splitting pattern that is consistent with a bridging hydride ligand at the Rh–Rh edge. Thus, the triplet of triplets at δ = -14.66 ppm (J(Rh,H) = 30.0 Hz and ^3J(P,H) = 7.2 Hz) should correspond to the *trans*-**8a** isomer (10 %).

The dynamic behaviour of the hydride ligand in **8** has been investigated by NMR spectroscopy. Unexpectedly, the only observed exchange cross-peaks in the ^{1}H–^{1}H NOESY spectrum (C_6D_6) was between the resonances at δ = -14.66 and -20.07 ppm that correspond to the isomers *trans*-**8a** and *cis*-**8b**, respectively. This observation is compatible with a static bridging hydride ligand in the *trans*-**8b** isomer and the equilibrium *trans*-**8a** ⇆ *cis*-**8b** as a consequence of the mobility of the hydride ligand (Scheme 3).

Discussion

Synthesis of trinuclear hydrido-sulfido clusters. The deprotonation of bis-hydrosulfido dinuclear complexes, [Rh(μ-SH){P(OPh)$_3$}$_2$]$_2$ and [Rh(μ-SH)(CO)(PPh$_3$)]$_2$, in the presence of d^8 rhodium or iridium metal fragments provides access to trinuclear hydrido-sulfido clusters with the core [M$_3$(μ-H)(μ$_3$-S)$_2$]. The deprotonation of [Rh(μ-SH){P(OPh)$_3$}$_2$]$_2$ by triethylamine in the presence of chloro-bridge dinuclear complexes [{M(μ-Cl)(diolef)}$_2$] (M = Rh, Ir) gave the clusters [Rh$_2$M(μ-H)(μ$_3$-S)$_2${P(OPh)$_3$}$_4$(diolef)] (**1**-**4**). The deprotonation can be also accomplished by using the methoxo-bridged dinuclear complexes [{M(μ-OMe)(cod)}$_2$] (M = Rh, Ir) although the reaction with the iridium complex is unselective and gave a mixture of several trinuclear clusters from which the unexpected cluster [RhIr$_2$(μ-H)(μ$_3$-S)$_2${P(OPh)$_3$}$_2$(cod)$_2$] (**5**) was isolated.

The bis-hydrosulfido complex [Rh(μ-SH)(CO)(PPh$_3$)]$_2$ can be also deprotonated by using mononuclear acetylacetonato complexes [M(acac)(diolef)] (M = Rh, Ir) to give the clusters [Rh$_3$(μ-H)(μ$_3$-S)$_2$(CO)$_2$(PPh$_3$)$_2$(diolef)] (**6**-**7**) and [Rh$_2$Ir(μ-H)(μ$_3$-S)$_2$(CO)$_2$(PPh$_3$)$_2$(cod)] (**8**). In contrast, [Rh(μ-SH){P(OPh)$_3$}$_2$]$_2$ failed to react with this type of complexes which is in

agreement with the lower acidity of their hydrosulfido ligands compared to the carbonyl-triphenylphosphine analogue.[18]

The clean synthesis of trinuclear hydrido-sulfido clusters from $[Rh(\mu\text{-}SH)(CO)(PPh_3)]_2$ and [M(acac)(diolef)] suggest that the formation of the clusters could involve the additive deprotonation[14g] of a hydrosulfido ligand to give trinuclear hydrosulfido-sulfido intermediates $[Rh_2M(\mu_3\text{-}SH)(\mu_3\text{-}S)(CO)_2(PR_3)_2(diolef)]$ (not observed by spectroscopic means) that collapse to the hydrido-sulfido clusters $[Rh_2M(\mu\text{-}H)(\mu_3\text{-}S)_2(CO)_2(PR_3)_2(diolef)]$ by a intramolecular proton transfer.

Hydride mobility in hydrido-sulfido clusters. Some of the trinuclear hydrido-sulfido clusters described in this work exhibit a dynamic behaviour as a consequence of the hydride migration between the edges of the metal triangle with the simultaneous movement of the Rh–Rh bond.

It is generally assumed that hydride fluxionality in trinuclear clusters occurs through a sequence of migrations involving the movement of a single bridging hydride ligand from one metal-metal vector to an adjacent unbridged edge.[28] However, DFT calculations on the model compound $[Rh_3(\mu\text{-}H)(\mu_3\text{-}S)_2(PH_3)_4(cod)]$ (**1'**) have demonstrated that the hydride migration around the bipiramidal-trigonal $[Rh_3S_2]$ core involves a μ_3-sulfido bridging ligand through the hydrosulfido-sulfido intermediate $[Rh_3(\mu_3\text{-}SH)(\mu_3\text{-}S)(PH_3)_4(cod)]$ (**1c'**). This species, that has been also proposed to participate in the formation of the clusters, is as a 48 valence electrons aggregate composed of 16-electron configuration Rh^I centers. Interestingly, the average experimental energy barriers values determined by 2D EXSY NMR for clusters **1**-**3** and **5** (Table 2) show good agreement with the ones theoretically calculated of $\Delta G_1^{\#}$ (Ts_a) = 75 kJ mol^{-1} and $\Delta G_{-1}^{\#}$ (Ts_b) = 67 kJ mol^{-1} for the model compound (Figure 6). On the other hand, the molecular structure of cluster **1** shows that the bridging hydride ligand is located at the Rh_P–Rh_P edge which is also in agreement with the theoretical calculations as this isomer,

1a', is 15.4 kJ mol^{-1} more stable than the isomer **1b'** where the hydride ligand bridges the Rh_P–Rh_{cod} edge.

The scope of the hydride migration phenomenon seems to be determined both by the metal composition of the cluster and the auxiliary ligands on the rhodium metal fragments. The influence of the ancillary ligands on the metal framework becomes evident in the dynamic $[Rh_3(\mu\text{-}H)(\mu_3\text{-}S)_2\{P(OPh)_3\}_4(cod)]$ (**1**) and static $[Rh_3(\mu\text{-}H)(\mu_3\text{-}S)_2(CO)_2(PPh_3)_2(cod)]$ (**6**) clusters with the bridiging hydride ligand located at the $Rh_{CO/P}$–$Rh_{CO/P}$ edge in the latter. Thus, the presence of strong π-acceptor ligands (CO) in **6** stabilizes the **a**-type isomer and, as result, the cluster is static. On the other hand, in contrast with **1**, the cluster $[Rh_2Ir(\mu\text{-}H)(\mu_3\text{-}S)_2\{P(OPh)_3\}_4(cod)]$ (**4**) is static with the hydride ligand at the Rh–Ir edge which is in full agreement with the structure found in the solid state. In this case, the easiest oxidation of the Ir(I) centers to Ir(II)[35] and the stronger Ir–H bonds[36] could account for the superior stability of the **b**-type isomer in **4**. Finally, the dynamic behaviour of the cluster $[RhIr_2(\mu\text{-}H)(\mu_3\text{-}S)_2\{P(OPh)_3\}_2(cod)_2]$ (**5**), with a $[RhIr_2]$ metal core, indicates a small energy difference between the **a** and **b**-type isomers with the hydride ligand at the Ir–Ir and Rh–Ir edges, respectively.

The dynamic behaviour of cluster $[Rh_2Ir(\mu\text{-}H)(\mu_3\text{-}S)_2(CO)_2(PPh_3)_2(cod)]$ (**8**) deserves further comments. The cluster exists as three isomers that arise from the disposition of the PPh_3 ligands in the cluster (*cis* and *trans*) and the location of the hydride ligand. As expected, the major isomers are *cis*-**8b** (22 %) and *trans*-**8b** (68 %) (figure 7) with the hydride ligand at the Rh–Ir edge. The minor isomer corresponds to *trans*-**8a** (10 %) although the *cis*-**8a** was not observed. Interestingly, the ^1H–^1H NOESY indicated a static bridging hydride ligand in *trans*-**8b** and the existence of the equilibrium *trans*-**8a** ⇆ *cis*-**8b** as a consequence of the mobility of the hydride ligand. Thus, the migration of the hydride ligand between the Rh–Rh and Rh–Ir edges also involves the *cis*-*trans* isomerization that is an indication of an exchange pathway

through a turnstile mechanism. The migration of the bridging hydride ligand to an equatorial terminal position results in a five-coordinated rhodium center that undergoes clockwise or anticlockwise turnstile rotation to allow the migration of the hydride ligand to the adjacent edge of the trimetallic core. Unexpectedly, the experimental energy barriers for this process determined by 2D EXSY NMR, $\Delta G_1^{\#} = 69.8$ kJ mol^{-1}, and $\Delta G_{-1}^{\#} = 71.6$ kJ mol^{-1} (Table 2), are very similar to those determined in clusters having triphenylphosphite as auxiliary ligands. The turnstile rotation of the fragment "RhH{P(OPh)$_3$}$_2$" is hindered by the presence of two bulky phosphite ligands favouring the hydride migration via a hydrosulfido intermediate. Obviously, the turnstile rotation of the "RhH(CO)(PPh$_3$)" requires much less energy because of the presence of only a bulky triphenylphosphine ligand. In addition, the presence of strong π-acceptor carbonyl ligands in **8** probably reduces the electronic density on the sulfido ligands making the hydride migration through sulphur less favourable in this case.

Dynamic hydrido-sulfido clusters as molecular models for the hydrogen migration on metal sulfide hydrotreating catalysts. Hydrotreating comprises a variety of catalytic hydrogenation processes that aim at reducing the heteroatom content of petroleum feedstocks. Molybdenum sulfides promoted by nickel (or cobalt) have been widely used as hydrotreating catalysts for the removal of sulfur, nitrogen, and other impurities from oil fractions.[1d, 37] Hydrotreating reactions require the activation of hydrogen on the catalyst surface and the subsequent reactions between hydrogen species and organic molecules.[38]

Theoretical investigations on the adsorption and dissociation of hydrogen both on promoted and unpromoted MoS_2 surfaces show that molecular hydrogen dissociates heterolytically leading to the formation of Mo–H and Mo–SH functionalities.[39] The presence of –SH groups on molybdenum-based catalysts has been established by many spectroscopic studies, however there is no experimental evidence supporting the existence of Mo–H groups, although such species have been found on other sulfide phases upon hydrogenation.[40] H–D isotopic

exchange between H_2 and D_2 in the presence of molybdenum sulfide catalysts indicates that the hydrogen species resulting from the heterolytic hydrogen activation on the catalyst surface, –SH and Mo–H, are highly mobile on the surface and can recombine to form molecular hydrogen.[41]

It has been determined that the activation energies for the surface migration processes are smaller than that for the initial dissociation process, which indicates the highly dynamic nature and mobility of surface hydrogen species. In particular, the migration of a hydrogen from Mo–H to a sulfur atom has a low energy barrier and the energies associated to the Mo–H and S–H bonds are close which could explain the low concentration of Mo–H groups on the catalyst surface.[42]

The modelling of the dihydrogen activation on transition metal sulfide catalysts by organometallic complexes has demonstrated that sulfido ligands can assist the heterolytic splitting of dihydrogen to produce hydrosulfido complexes. In fact, several ruthenium, titanium, rhodium and iridium hydrido-hydrosulfido complexes have been obtained by reaction of sulfido metal complexes with dihydrogen.[43] In contrast, there is not experimental evidence at molecular level for the sulphur-assisted hydride migration on sulfido clusters. Thus, the dynamic behaviour of the hydrido-sulfido clusters $[Rh_3(\mu\text{-}H)(\mu_3\text{-}S)_2\{P(OPh)_3\}_4(diolef)]$, that involves the hydrogen migration from rhodium to sulphur with a switch from hydride to proton character, models the hydrogen mobility on metal sulfide hydrotreating catalyst by interconversion between surface metal hydrides and –SH.

Conclusions

The bis(hydrosulfido)-bridged dinuclear complexes $[Rh(\mu\text{-}SH)\{P(OPh)_3\}_2]_2$ and $[Rh(\mu\text{-}SH)(CO)(PR_3)]_2$ are suitable precursors for the synthesis of homo- and heterotrinuclear sulfido clusters with the core $[M_3(\mu\text{-}H)(\mu_3\text{-}S)_2]$ (M = Rh, Ir). The deprotonation of a

hydrosulfido ligand in the presence of d^8 rhodium or iridium metal fragments results in the formation of intermediate hydrosulfido-sulfido clusters with the core $[M_3(\mu_3\text{-}SH)(\mu_3\text{-}S)_2]$ that are precursors of the hydrido-sulfido clusters by an intramolecular proton transfer. Some trinuclear hydrido-sulfido clusters exhibit a dynamic behaviour due to the hydride migration between the edges of the metal triangle. The mobility of the hydride ligand is influenced both by the metal composition of the cluster and the auxiliary ligands on the rhodium metal fragments. The presence of bulky ligands makes the classical turnstile mechanism improbable and theoretical calculations have demonstrated that an alternative mechanism involving the direct transfer of the hydride to a sulfido ligand, between the different bridging positions in the bipiramidal-trigonal core, is feasible. The calculated energy barriers for this process compare well with those determined by two-dimensional exchange spectroscopy. The movement of the hydride ligand in the clusters is consistent with a proton migrating over the electronic density at the rhodium centers on the edges and the sulfido ligand. Interestingly, this mechanism is relevant to the possible pathways for the hydrogen diffusion on solid surfaces and this kind of clusters could be considered as molecular models for the hydrogen migration on metal sulfide hydrotreating catalysts.

Experimental Section

General methods All manipulations were performed under a dry argon atmosphere using Schlenk-tube techniques. Solvents were obtained from a Solvent Purification System (Innovative Technologies). ^1H and $^{31}P\{^1H\}$ NMR spectra were recorded on a Bruker Avance 300 (300.13 and 121.50 MHz), Bruker Avance 400 MHz (400.13 and 161.99 MHz) and Bruker Avance 500 MHz (500.13 and 202.45 MHz) spectrometers. Chemical shifts are reported in parts per million and referenced to $SiMe_4$ using the signal of the deuterated solvent (^1H) and 85% H_3PO_4 (^{31}P) as external reference, respectively. Full assignment of the

resonances was done by combination of $^{1}H–^{1}H$ COSY, $^{1}H–^{31}P$ HMBC and $^{1}H\{^{31}P\}$ NMR spectroscopy techniques. IR spectra were recorded in solution on a Perkin-Elmer Spectrum One spectrometer using a cell with NaCl windows. Elemental C, H and N analysis were performed in a Perkin-Elmer 2400 CHNS/O microanalyzer. Mass spectra were recorded in a VG Autospec double-focusing mass spectrometer operating in the FAB^{+} mode. Ions were produced with the standard Cs^{+} gun at ca. 30 Kv, 3-nitrobenzyl alcohol (NBA) was used as matrix. Electrospray mass spectra (ESI–MS) were recorded on a Bruker MicroTof-Q using sodium formiate as reference. Standard literature procedures were used to prepare the starting materials [{Rh(μ-Cl)(diolef)}$_2$] (diolef = cod,[44] nbd,[45] tfb,[46]) and [{Ir(μ-Cl)(cod)}$_2$].[47] The acetylacetonato complexes [Rh(acac)(diolef)] (diolef = cod, nbd)[48] and [Ir(acac)(cod)],[49] and the complexes [{M(μ-OMe)(cod)}$_2$] (M = Rh, Ir)[50] were prepared according to the previously reported methods. [Rh(μ-SH){P(OPh)$_3$}$_2$]$_2$ and [Rh(μ-SH)(CO)(PPh$_3$)]$_2$ were prepared following the synthetic procedure recently described.[18]

Synthesis of [Rh$_3$(μ-H)(μ$_3$-S)$_2$\{P(OPh)$_3$\}$_4$(cod)]·CH$_2$Cl$_2$ (1·CH$_2$Cl$_2$). *Method A*. To a yellow solution of [Rh(μ-SH){P(OPh)$_3$}$_2$]$_2$ (0.120 g, 0.079 mmol) in benzene (2 mL), was added solid [Rh(μ-OMe)(cod)]$_2$ (0.019 mg, 0.039 mmol) to give a bright-red solution which was stirred for 2 hours. The solvent was evaporated under vacuum and the residue washed with *n*-hexane (2 x 10 mL) and dissolved in CH_2Cl_2 (1 mL). The resulting brown solution was layered with *n*-hexane (8 mL) at RT for 24 h to give dark red crystals, which were filtered off, washed with pentane and dried under vacuum (0.090 g, 63 %). *Method B*. To a solution of [Rh(μ-SH){P(OPh)$_3$}$_2$]$_2$ (0.100 g, 0.066 mmol) in benzene (2 mL) was added NEt_3 (100 μL, 0.719 mmol, ρ = 0.728 g mL^{-1}). The solution was stirred for 15 min and then reacted with solid [Rh(μ-Cl)(cod)]$_2$ (0.016 g, 0.033 mmol) to give a deep red solution which was stirred for 2 hours. The solvent was evaporated under vacuum and the residue dissolved in CH_2Cl_2 (1 mL). The resulting dark red solution was layered with *n*-hexane (8 mL) and kept at 258 K to

give dark red microcrystals, which were filtered off, washed with pentane and dried in vaccuo (0.098 g, 82 %).^{1}H NMR (300.13 MHz, C_6D_6, 298 K): δ = 7.59 (d), 7.43 (d), 7.37 (d), 7.14 – 7.03 (set of m), 6.91 (t) (OPh), 4.53 (br) (**1b**), 4.08 (br) (**1a**), 3.77 (br) (**1b**) (=CH, cod), 2.16 (m), 2.04 (m), 1.85 (m) (>CH_2, cod), -13.75 (ddt, *J*(Rh,H) = 31.5 Hz, *J*(Rh,H) = 27.7 Hz, ^{2}J(P-H) = 6.9 Hz; Rh-H) (**1b**), -14.37 (tq, *J*(Rh,H) = 29.7 Hz, ^{2}J(P,H) = 6.9 Hz; Rh-H) (**1a**); ^{31}P{^{1}H} NMR (121.50 MHz, C_6D_6, 298 K): δ = 112.70 (br d, *J*(Rh,P) = 264 Hz); MS (FAB+, CH_2Cl_2): m/z (%): 1722 (15) $[M]^+$, 1412 (10) $[M - P(OPh)_3]^+$, 1302 (10) $[M - cod - P(OPh)_3 - H]^+$, 1101 (100) $[M - 2P(OPh)_3 - H]^+$; MS (ESI–, THF/CH_3CN): m/z (%): 1721.1 $[M - H]^-$; elemental analysis calcd (%) for $C_{81}H_{75}Cl_2O_{12}P_4Rh_3S_2$ (1808.12): C 53.81, H 4.18, S 3.55; found: C 53.49, H 4.19, S 3.39.

Synthesis of [Rh$_3$(μ-H)(μ$_3$-S)$_2${P(OPh)$_3$}$_4$(nbd)] (2). NEt_3 (100 μL, 0.719 mmol, ρ = 0.728 g mL^{-1}) was added to a solution of [{Rh(μ-SH)(P(OPh)$_3$)$_2$}$_2$] (0.100 g, 0.066 mmol) in benzene (3 mL). The solution was stirred for 15 min. and then reacted with solid [Rh(μ-Cl)(nbd)$_2$]$_2$ (0.015 g, 0.033 mmol) to give a red-brown solution that was stirred for 2 hours. The solution was brought to dryness under vacuum and the residue dissolved in CH_2Cl_2 (1 mL). Slow diffusion of *n*-hexane (8 mL) at 258 K gave the compound as orange microcrystals which were filtered off, washed with pentane and dried in vaccuo (0.079 g, 70 %). ^{1}H NMR (300.13 MHz, CD_2Cl_2, 223 K): δ = 7.41 (m), 7.06 (m), 6.91 (t) (OPh), 3.76 (br) (**2a** and **2b**), 3.43 (br) (**2b**) (=CH, nbd), 3.05 (br) (**2b**), 2.98 (br) (**2a**) (CH, nbd), 1.27 (m, >CH_2, nbd) (**2a** and **2b**), -13.77 (ddt, *J*(Rh,H) = 31.4 Hz, *J*(Rh,H) = 24.2 Hz, ^{2}J(P,H) ≈ 8.5 Hz; Rh-H) (**2b**), -14.80 (tq, *J*(Rh,H) = 30.1 Hz, ^{2}J(P,H) ≈ 8.5 Hz; Rh-H) (**2a**). ^{31}P{^{1}H} NMR (121.50 MHz, CD_2Cl_2, 223 K): δ = 113.04 (br d, *J*(Rh,P) = 253 Hz), 112.07 (br dd, *J*(Rh,P) = 279 Hz, ^{3}J(P,P) = 12 Hz) (**2b**), 111.58 (br d, *J*(Rh,P) = 263 Hz) (**2a**). MS (ESI–, THF/CH_3CN): m/z (%): 1705.1 $[M - H]^-$; elemental analysis calcd (%) for $C_{79}H_{69}O_{12}P_4Rh_3S_2$ (1707.14): C 55.58, H 4.07, S 3.76; found: C 55.16, H 4.71, S 3.67.

Synthesis of $[Rh_3(\mu\text{-}H)(\mu_3\text{-}S)_2\{P(OPh)_3\}_4(tfb)]$ (3). $[Rh(\mu\text{-}SH)\{P(OPh)_3\}_2]_2$ (0.100 g, 0.066 mmol), $[Rh(\mu\text{-}Cl)(tfb)_2]_2$ (0.024 g, 0.033 mmol) and NEt_3 (100 μL, 0.719 mmol, ρ = 0.728 g mL^{-1}) were reacted in benzene (3 mL), following the procedure described for compound **2**, to give an orange-red suspension in 2 hours. The solvent was removed under vacuum and the residue dissolved in CH_2Cl_2 (1 mL). Slow diffusion of *n*-hexane (8 mL) at 258 K gave the compound as orange-brown microcrystals, which were filtered off, washed with pentane and dried under vacuum (0.068 g, 56%).^{1}H NMR (400.13 MHz, CD_2Cl_2, 193 K): δ = 7.20 (m), 7.10 (m), 6.96 (m) (OPh), 4.65 (br) (**3a** and **3b**) (CH tfb), 3.53 (br) (**3b**), 3.10 (br) (**3a**), 2.70 (br) (**3b**) (=CH, tfb), -14.25 (ddt, *J*(Rh,H) = 32.4 Hz, *J*(Rh,H) = 22.4 Hz, ^2J(P,H) < 5 Hz, Rh-H) (**3b**), -14.83 (tq, *J*(Rh,H) = 30.0 Hz, ^2J(P,H) < 5 Hz, Rh-H) (**3a**). $^{31}P\{^1H\}$ NMR (161.99 MHz, CD_2Cl_2, 193 K): δ = 112.75 (br d, *J*(Rh,P) = 249 Hz), 111.89 (br d, *J*(Rh,P) = 263 Hz) (**3b**), 112.44 (br d, *J*(Rh,P) = 278 Hz) (**3a**); MS (ESI–, THF/CH_3CN): m/z (%): 1839.1 [M – H]$^-$; elemental analysis calcd (%) for $C_{84}H_{67}F_4O_{12}P_4Rh_3S_2$ (1841.17): C 54.80, H 3.67, S 3.48; found: C 54.64, H 3.91, S 3.56.

Synthesis of $[Rh_2Ir(\mu\text{-}H)(\mu_3\text{-}S)_2\{P(OPh)_3\}_4(cod)]\cdot CH_2Cl_2$ (4·CH_2Cl_2). $[\{Rh(\mu\text{-}SH)(P(OPh)_3)_2\}_2]$ (0.080 g, 0.053 mmol), $[Ir(\mu\text{-}Cl)(cod)]_2$ (0.018 g, 0.027 mmol) and NEt_3 (100 μL, 0.719 mmol, ρ = 0.728 g mL^{-1}) were reacted in benzene (3 mL), following the procedure described for compound **2**, to give a dark red solution in 2 hours. The solvent was evaporated under vacuum and the residue dissolved in CH_2Cl_2 (1 mL). Slow diffusion of *n*-hexane (8 mL) at 258 K gave the compound as dark red crystals, which were filtered off, washed with pentane and dried under vacuum (0.068 g, 68%). ^{1}H NMR (300.13 MHz, C_6D_6, 298 K): δ = 7.40 (d), 7.23 (d), 6.94 (m), 6.76 (t) (OPh), 4.18 (br), 3.53 (br) (=CH, cod), 2.31 (m), 1.93(m), 1.62 (m) (>CH_2, cod), -20.09 (br d, *J*(Rh,H) = 24.3 Hz, Rh-H); $^{31}P\{^1H\}$ NMR (121.50 MHz, C_6D_6, 298 K): δ = 113.81 (dm, *J*(Rh,P) = 274 Hz), 112.48 (dm, *J*(Rh,P) = 275

Hz); MS (FAB+, CH_2Cl_2): m/z (%): 1812 (70) $[M]^+$, 1501 (25) $[M - P(OPh)_3]^+$, 1191 (100) $[M - 2P(OPh)_3]^+$, 1084 (40) $[M - 2P(OPh)_3 - cod]^+$. MS (ESI–, THF/CH_3CN): m/z (%): 1811.2 $[M - H]^-$; elemental analysis calcd (%) for $C_{81}H_{75}Cl_2IrO_{12}P_4Rh_2S_2$ (1897.43): C 51.27, H 3.98, S 3.38; found: C 51.23, H 4.01, S 3.35.

Synthesis of $[RhIr_2(\mu\text{-}H)(\mu_3\text{-}S)_2\{P(OPh)_3\}_2(cod)_2]$ (5). $[Rh(\mu\text{-}SH)\{P(OPh)_3\}_2]_2$ (0.200 g, 0.132 mmol) and $[Ir(\mu\text{-}OMe)(cod)]_2$ (0.088 g, 0.132 mmol) were reacted in benzene (3 mL) for 2 h to give a dark red solution. The solvent was removed under vacuum and the residue dissolved in CH_2Cl_2 (3 mL) and layered with *n*-hexane (10 mL) at RT to give dark red crystals of compound **4**. The crystals were separated by filtration and the solution concentrated under vacuum to give a red-brown suspension. The precipitation was complete by further addition of *n*-hexane and the solid was isolated by filtration. Crystallization from CH_2Cl_2/*n*-hexane gave the compound as a red-brown microcrystalline solid that was filtered, washed with cold *n*-hexane and dried under vacuum (0.075 g, 41%, based on Ir). ^1H NMR (300.13 MHz, C_6D_6, 298 K): δ = 7.47 (d), 7.40 (t), 7.21 (m), 7.01 – 6.73 (set of m) (OPh), 4.84 (br), 4.53 (br) (**5b**), 4.26 (br), 4.10 (br) (**5a**), 3.93 (br), 3.68 (br) (**5b**) (=CH, cod), 2.25 (m), 1.99 (m), 1.77 (m) (>CH_2, cod), -20.90 (br d, J(Rh,H) = 19.5 Hz, Rh-H) (**5b**), - 21.74 (br s, Rh-H) (**5a**); $^{31}P\{^1H\}$ NMR (121.50 MHz, C_6D_6, 298 K): δ = 120.07 (d, J(Rh,P) = 281 Hz) (**5b**), 117.62 (d, J(Rh,P) = 284 Hz) (**5a**). MS (ESI–, THF/CH_3CN): m/z (%): 1387.1 $[M - H]^-$; elemental analysis calcd (%) for $C_{52}H_{55}Ir_2O_6P_2RhS_2$ (1389.42): C 44.95, H 3.99, S 4.61; found: C 44.85, H 4.02, S 4.53.

Synthesis of $[Rh_3(\mu\text{-}H)(\mu_3\text{-}S)_2(CO)_2(PPh_3)_2(cod)]$ (6). $[Rh(\mu\text{-}SH)(CO)(PPh_3)]_2$ (0.080 g, 0.094 mmol) and [Rh(acac)(cod)] (0.029 g, 0.094 mmol) were reacted in CH_2Cl_2 (10 mL) at 258 K for 45 minutes to give a deep red-brown solution. The solvent was removed under vacuum and the residue dissolved in diethyl ether (5 mL). The stirring of the solution induced the crystallization of the compound as a garnet microcrystalline solid. The suspension was

concentrated and cooled to 258 K. The solid was collected by filtration, washed with cold diethyl ether (2 x 2 mL) and then vacuum-dried (0.072 g, 72 %). ^{1}H NMR (300.13 MHz, C_6D_6, 298 K): δ = 8.23 – 7.77 (m, 12H), 7.08 – 6.99 (m, 12H), 6.99 – 6.95 (m, 6H) (PPh_3), 4.62 (m, 2H), 4.53 (m, 2H) (=CH cod), 2.36 (m, 2H), 2.22 (m, 2H), 2.06 (m, 2H), 2.00 (m, 2H) (>CH_2 cod), -13.87 (tt, *J*(Rh,H) = 31.5 Hz, *J*(P,H) = 5.4 Hz, Rh-H). ^{31}P{^{1}H} NMR (121.50 MHz, C_6D_6, 298 K): δ = 34.15 (d, *J*(Rh,P) = 152 Hz); MS (ESI+, THF/CH_3CN): m/z (%): 1061 $[M - H]^+$, 1033 $[M - H - CO]^+$; IR (CH_2Cl_2): ν = 1984 (sh), 1969 (s) cm^{-1} (CO); elemental analysis calcd (%) for $C_{46}H_{43}O_2P_2Rh_3S_2$ (1062.63): C 51.99, H 4.08, S 6.03; found: C 51.45, H 4.01, S 6.08.

Synthesis of [$Rh_3(\mu$-H)(μ_3-S)$_2$(CO)$_2$(PPh_3)$_2$(nbd)] (7). [Rh(μ-SH)(CO)(PPh_3)]$_2$ (0.160 g, 0.188 mmol) and [Rh(acac)(nbd)] (0.056 g, 0.188 mmol) were reacted in CH_2Cl_2 (10 mL) at 258 K for 20 minutes to give a deep red solution. Work up as describe above for compound **6** gave the compound as a garnet microcrystalline solid (0.148 g, 75%). ^{1}H NMR (300.13 MHz, C_6D_6, 298 K): δ = 7.82 – 7.76 (m, 12H), 7.07 – 7.01 (m, 18H) (PPh_3), 4.25 (m, 4H) (=CH), 3.49 (m, 2H) (CH), 1.28 (m, 2H) (>CH_2) (nbd), -13.74 (tt, *J*(Rh,H) = 32.4 Hz, *J*(P,H) = 4.2 Hz, Rh-H). ^{31}P{^{1}H} NMR (121.50 MHz, C_6D_6, 298 K): δ = 34.45 (d, *J*(Rh,P) = 153 Hz); MS (ESI+, THF/CH_3CN): m/z (%): 1045 $[M - H]^+$, 1017 $[M - H - CO]^+$; IR (CH_2Cl_2): ν = 2000 (sh), 1983 (s) cm^{-1} (CO); elemental analysis calcd (%) for $C_{45}H_{39}O_2P_2Rh_3S_2$ (1046.59): C 51.64, H 3.76, S 6.13; found: C 51.55, H 3.68, S 6.10.

Synthesis of [$Rh_2Ir(\mu$-H)(μ_3-S)$_2$(CO)$_2$(PPh_3)$_2$(cod)] (8). [Rh(μ-SH)(CO)(PPh_3)]$_2$ (0.080, 0.094 mmol) and [Ir(acac)(cod)] (0.038 g, 0.094 mmol) were reacted in tetrahydrofurane (5 mL) for 5 hours to give a deep red solution. The solvent was removed under vacuum and the residue stirred in a 3:1 diethyl ether/tetrahydrofurane mixture (4 mL) at 258 K. The red-garnet solid obtained was collected by filtration, washed with cold diethyl ether (3 x 3 mL) and dried

under vacuum (0.095 g, 88 %). ^{1}H NMR (400.13 MHz, C_6D_6, 298 K): δ = 7.95 – 7.71 (m), 7.11 – 7.00 (m) (PPh_3), 5.10 (br) (*cis*-**8b**), 4.74 (br), 4.66 (br) (*trans*-**8b**), 4.59 (br) (*cis*-**8b**), 4.41 (br) (*trans*-**8a**), 4.27 (*cis*-**8b** and *trans*-**8b**), 3.70 (br) (*trans*-**8b**), 3.38 (br) (*cis*-**8b**), 2.55 (m), 2.32 (m), 2.14 (m), 2.11 (m), 1.94 (m), 1.78 (m) (>CH_2 cod), -14.66 (tt, J(Rh,H) = 30.0 Hz, ^{2}J(P,H) = 7.2 Hz, Rh-H) (*trans*-**8a**), -20.07 (d, J(Rh,H) = 23.6 Hz, Rh-H) (*cis*-**8b**), -20.54 (d, J(Rh,H) = 23.6 Hz, Rh-H) (*trans*-**8b**); ^{31}P{^{1}H} NMR (161.99 MHz, C_6D_6, 298 K): δ = 36.65 (dd, J(Rh,P) = 163 Hz, ^{3}J(P,P) = 13 Hz), 34.09 (dd, J(Rh,P) = 163 Hz, ^{3}J(P,P) = 13 Hz) (*trans*-**8b**), 36.30 (br d, J(Rh,P) = 160 Hz), 34.54 (br d, J(Rh,P) = 164 Hz) (*cis*-**8b**), 35.6 (d, J(Rh,P) ≈ 160 Hz) (*trans*-**8a**); MS (ESI–, THF/CH_3CN): m/z (%): 1149 [M – H]$^{-}$; IR (C_6H_6): ν = 1995 (sh), 1985 (s), 1976 (s) cm^{-1} (CO); elemental analysis calcd (%) for $C_{46}H_{43}IrO_2P_2Rh_2S_2$ (1151.94): C 47.96, H 3.76, S 5.57; found: C 47.80, H 3.70, S 5.42.

Experimental procedure for the determination of the kinetic parameters. Rate constants (k_1 and k_{-1}/s^{-1}) for the equilibrium **a** ⇆ **b** in clusters **1-3**, **5** and **8** were obtained from the 2D EXSY spectra using a gradient selected NOESY program from Bruker (noesygpph). All spectra were recorded at 500.13 MHz with mixing times (t_m) optimized for 300 K. The spectra were recorded with a sweep of 33 ppm, 2048 data points in the $F2$ direction, 512 increments in the $F1$, eight transients per increment, acquisition time (t_{ac}) of 75 ms, and relaxation delay (d_1) optimized following the equation:

$$3\,T_1 = t_{ac} + t_m + d_1$$

The spectra were apodized with a qsine function and zero filled. They were phased to give negative peaks along the diagonal. The baseline in $F1$ and $F2$ was corrected and then, all the spectra were phased using the phase sensitive method from Bruker.

The basis of the calculation of the kinetic data (k_1 and k_{-1}/s^{-1}) from the EXSY experiments is the integration of the cross-peaks amplitudes of the 2D EXSY spectra performed using the MestReC software.[24] The hydride resonances involved in the exchange process are

conveniently separated from the others in the NMR spectrum what allows the application of the MestReC approach. Two different 2D EXSY NMR spectra were acquired and processed under identical conditions, temperature, number of scans, etc. for each sample. The first spectrum is an EXSY experiment acquired at the optimized mixing time (t_m), and the second an EXSY experiment acquired at 0 or very short mixing time (reference experiment). The amplitudes (intensities) of the signals in exchange, A_{ij}, were quantified for both spectra, both diagonal and cross peaks in the first spectrum and only the diagonal peaks, A(0), in the reference spectrum, as there is no cross peaks due to the absence of magnetization exchange (see Supporting information).

The longitudinal relaxation times T_1 were measured using the inversion-recovery method with the appropriate pulse sequence. For a system with two exchange sites, i and j, of equal relaxation time T_1, the optimum value of the mixing time (t_m) to maximize the cross-peaks intensities can be calculated using the following equation where k_{ij}, and k_{ji} are the exchange rate constants between them.[23, 51]

$$t_m = \left(1/k_{ij}+k_{ji}\right)\left[\ln\left(1+\left(k_{ij}+k_{ji}\right)T_1\right)\right]$$

An adequate approximation for the optimum mixing time (t_m) derived from a statistical analysis is the following expression.[52]

$$t_m \approx 1/\left[T_1^{-1}+k_{ij}+k_{ji}\right]$$

The activation energies, $\Delta G_1^{\#}$ and $\Delta G_{-1}^{\#}$ ($kJ \cdot mol^{-1}$) were calculated from the chemical exchange rate constants obtained from ESXYCalc, k_1 and k_{-1}, using the Eyring equation.

Theoretical calculations. The calculations were performed with the Gaussian03 software package[53] at the density functional theory (DFT) using the B3LYP functional. A set of model systems were used, obtained by replacing the phenyl groups on $P(OPh)_3$ ligands with H atoms. All were fully optimized without any symmetry restriction. The basis set employed

was 6-31G** for all the atoms but the Rh atoms, where the LANL2DZ pseudopotential an associated basis set were used. The stationary states, both minima and transition states, were characterized by frequency calculations and the imaginary frequency of the transition states was visually checked to assess its correct relation with the related minima. Cartesian coordinates, absolute energies, and graphical representation including selected geometrical parameters for the stationary states are provided in the Supporting information.

Crystal structure determination of $[Rh_3(\mu\text{-}H)(\mu_3\text{-}S)_2\{P(OPh)_3\}_4(cod)]$ (1) and $[Rh_2Ir(\mu\text{-}H)(\mu_3\text{-}S)_2\{P(OPh)_3\}_4(cod)]$ (4). Single crystals for the X-ray diffraction study of **1** and **4** were grown by slow diffusion of *n*-hexane into dichloromethane solutions of the clusters at 258 K. Intensity data for both molecules were collected at low temperature (100(2) K) on a Bruker SMART APEX CCD area detector diffractometer, using graphite-monochromated $Mo_{K\alpha}$ radiation (λ = 0.71073 Å) and narrow ω scans (0.3º). Cell parameters were refined from the observed setting angles and detector positions of strong reflections (6135 reflns, $2\theta \leq 46.8º$ for **1** and 7873 reflns, $2\theta \leq 50.2º$ for **4**). Data were processed using SAINT, including corrections for Lorentz and polarization effects;[54] multiscan absorption corrections were also applied with SADABS.[55]

The structures were solved by direct methods [SHELXS86[56] (**1**) and SIR2002[57] (**4**)] and completed by successive difference Fourier synthesis. Refinement, by full-matrix least-squares on F^2, was carried out with SHELXL97,[58] including in both structures all non-disordered non-hydrogen atoms with anisotropic displacement parameters. Both crystal structures showed similar difficulties in the refinement procedure and were processed in an analogous way. As it is common for phosphite ligands, some of the phenyl groups were observed disordered and were modeled on the base of two moieties with equal occupancy factors. Additionally a dichloromethane molecule was also observed disordered; again two moieties with complementary occupancies were include in the interpretation of the electron

density. Organic hydrogen atoms were included in the refinement from calculated positions only for the metal complexes and were refined as riding atoms. At this stage, in both cases, three significant residuals were observed in the different Fourier maps; they were interpreted as highly disordered *n*-hexane solvent molecules having partial occupancy [0.5 (**1**) and 0.25 (**4**)]. Potential energy minimizations were carried out (HYDEX program[21]) to locate the hydride positions; values obtained were not very different for the three M-M bridging possible positions, but the lowest minima were clearly observed between Rh(1) and Rh(2) (**1**) and Rh(1) and Ir (**4**). No significant residual (all < 1.23 e/Å^3) was observed in the final Fourier maps.

Crystal data for 1: $C_{80}H_{73}O_{12}P_4Rh_3S_2 \cdot CH_2Cl_2 \cdot 0.5\ C_6H_{14}$, M_r = 1851.13, triclinic, space group *P*-1, red irregular block crystal 0.181 × 0.126 × 0.117 mm, a = 13.0073(7), b = 14.4878(7), c = 23.2534(12) Å, α = 88.046(1), β = 80.010(1), γ = 63.732(1)º, V = 3865.4(3) Å^3, Z = 2, ρ_{calcd}=1.590 g cm^{-3}, $\mu(Mo_{K\alpha})$ = 0.902 mm^{-1}. Semiempirical absorption correction (min & max trans. 0.854 and 0.902), 47387 measured reflections (1.57 ≤ θ ≤ 28.51º, senθ/λ ≤ 0.672 Å^{-1}), 17908 unique (R_{int} = 0.0510); number of data/restrains/parameters 17908/2/994; final R_1 = 0.0527 (13091 observed reflns. $I > 2\sigma(I)$), $wR2$ = 0.1206, S = 1.028 for all data.

Crystal data for 4: $C_{80}H_{73}IrO_{12}P_4Rh_2S_2 \cdot CH_2Cl_2 \cdot 0.25\ C_6H_{14}$, M_r = 1918.87, triclinic, space group *P*-1, dark red prismatic crystal 0.291 × 0.153 × 0.126 mm, a = 12.9766(6), b = 14.4980(7), c = 23.1396(12) Å, α = 88.7880(10), β = 80.4990(10), γ = 64.4080(10)º, V = 3866.3(3) Å^3, Z = 2, ρ_{calcd}=1.648 g cm^{-3}, $\mu(Mo_{K\alpha})$ = 2.407 mm^{-1}. Semiempirical absorption correction (min. & max. trans. 0.541 and 0.751), 44336 measured reflections (1.56 ≤ θ ≤ 26.64º, senθ/λ ≤ 0.631 Å^{-1}), 16024 unique (R_{int} = 0.0457); number of data/restrains/parameters 16024/1262/964; final R_1 = 0.0396 (13197 observed reflns. $I > 2\sigma(I)$), $wR2$ = 0.0842, S = 1.002 for all data.

CCDC-805268 (**1**) and CCDC-805269 (**4**) contain the supplementary crystallographic data for this paper. These data can be obtained free of charge from the Cambridge Crystallographic Data Centre via www.ccdc.cam.ac.uk/data_request/cif.

Acknowledgements. Financial support from Ministerio de Ciencia e Innovación (MICINN/FEDER) is gratefully acknowledged (Projects: CTQ2006-03973 and CTQ2009-08089).

References

[1] a) *Transition Metal Sulfur Chemistry: Biological and Industrial Significance* (Eds.: E. I. Stiefel, K. Matsumoto), ACS, Washington DC. **1996**; b) *Transition Metal Sulfides: Chemistry and Catalysis* (Eds.: T. Weber, R. Prins, R. A. van Saen), Kluver Academic, Dordrecht, **1997**; c) M. Brorson, J. D. King, K. Kiriakidou, F. Prestopino, E. Nordlander, In *Metal Cluster in Chemistry* (Eds.: P. Braunstein, L. A. Oro, P. R. Raithby), Wiley-VCH, Weinhein, **1999**, Vol. 2, Chapter 2.6; d) H. Topsøe, B. S. Clausen, F. E. Massoth, *Hydrotreating Catalysis Science and Technology*, Springer-Verlag, Berlin, **1996**, vol. 11.

[2] a) C. Tard, C. J. Pickett, *Chem. Rev.* **2009**, *109*, 2245–2274; b) J. C. Fontecilla-Camps, A.Volbeda, C. Cavazza, Y. Nicolet, *Chem. Rev.* **2007**, *107*, 4273–4303; c) D. J. Evans, C. J. Pickett, *Chem. Soc. Rev.* **2003**, *32*, 268–275; d) M. Y. Darensbourg, E. J. Lyon, J. J. Smee, *Coord. Chem. Rev*. **2000**, *206-207*, 533–561; e) H. Ogino, S. Inomata, H. Tobita, *Chem. Rev.* **1998**, *98*, 2093–2122; f) H. Beinert, R. H. Holm, E. Münck, *Science*, **1997**, *277*, 653–659.

[3] a) L. Wang, Y. Zhang, Y. Zhang, Z. Jiang, C. Li, *Chem. Eur. J.* **2009**, *46*, 12571–12575; b) A. Olivas, D. H. Galvan, G. Alonso, S. Fuentes*, Appl. Catal. A* **2009**, *352*, 10–16; c)

L. Zhang, P. Afanasiev, D. Li, Y. H. Shi, M. Vrinat, *C. R. Chim.* **2008**, *11*, 130–136; d) S. Eijsbouts, S. W. Mayo, K. Fujita, *Appl. Catal. A* **2007**, *322*, 58–66; e) L. Zhang, P. Afanasiev, D. Li, X. Y. Long, M. Vrinat, *Catal. Commun.* **2007**, *8*, 2232–2237; f) Y. Gochi, C. Ornelas, F. Paraguay, S. Fuentes, L. Alvarez, J. L. Rico, G. Alonso-Nunez, *Catal. Today* **2005**, *107*, 531–536.

[4] a) M. Hidai, Y. Mizobe, *Can. J. Chem.* **2005**, *83*, 358–374; b) L. A. Oro, M. A. Ciriano, J. J. Pérez-Torrente, M. A. Casado, M. A. F. Hernandez-Gruel, *C. R. Chim.* **2003**, *6*, 47–57; c) Llusar, R.; Uriel, S. *Eur. J. Inorg. Chem.* **2003**, 1271–1290; d) M. Hidai, S. Kuwata, Y. Mizobe, *Acc. Chem. Res.* **2000**, *33*, 46–52.

[5] a) J. P. Lang, S. J. Ji, Q. F. Xu, Q. Shen, K. Tatsumi, *Coord. Chem. Rev.* **2003**, *241*, 47–60; b) C. -M. Che, B. -H. Xia, J. -S. Hung, C. -K. Chan, Z.-Y.Zho, K. -K. Cheung, *Chem. Eur. J.* **2001**, *7*, 3998–4006; c) H.-W. Hou, X.-Q. Xin, S. Shi, *Coord. Chem. Rev.* **1996**, *153*, 25–56.

[6] a) Z. G. Ren, H. X. Li, G. F. Liu, W. H. Zhang, J. P. Lang, Y. Zhang, Y. L. Song, *Organometallics* **2006**, *25*, 4351–4357; b) T. Amitsuka, H. Seino, M. Hidai, Y. Mizobe, *Organometallics* **2006**, *25*, 3034–3039; c) Z.-G. Ren, H.-X. Li, G.-F. Liu,; W.-H. Zhang, J.-P. Lang, Y. Zhang, Y.-L. Song, *Organometallics* **2006**, *25*, 4351–4357; d) H. Seino, T. Kaneko, S. Fujii, M. Hidai, Y. Mizobe, *Inorg. Chem.* **2003**, *42*, 4585–4596.

[7] a) R. H. Molina, I. Kalinina, M. Sokolov, M. Clausen, J. G. Platas, C. Vicent, R. Llusar, *Dalton Trans.* **2007**, 550–557; b) A. G. Algarra, M. G. Basallote, M. Feliz, M. J. Fernández-Trujillo, E. Guillamón, R. Llusar, C. Vicent, *Inorg. Chem.* **2006**, *45*, 5576–5584; c) K. Herbst, L. Dahlenburg, M. Brorson, *Inorg. Chem*. **2004**, *43*, 3327–3328; d) R. Hernández-Molina, M. N. Sokolov, A. G. Sykes, *Acc. Chem. Res*. **2001**, *34*, 223–230; e) T. Shibahara, *Coord. Chem. Rev*. **1993**, *123*, 73–147.

[8] a) M. Peruzzini, I. de los Rios, A. Romerosa, *Prog. Inorg. Chem.* **2001**, *49*, 169–453; b)

S. Kubata, M. Hidai, *Coord. Chem. Rev.* **2001**, *213*, 211–305.

[9] H. Kato, H. Seino, Y. Mizobe, M. Hidai, *J. Chem. Soc., Dalton Trans.* **2002**, 1494–1499.

[10] a) K. Arashiba, H. Lizuka, S. Matsukawa, S. Kuwata, Y. Tanabe, M. Iwasaki, Y. Ishii, *Inorg. Chem*. **2008**, *47*, 4264–4274; b) K. Arashiba, S. Matsukawa, S. Kuwata, Y. Tanabe, M. Iwasaki, Y. Ishii, *Organometallics*, **2006**, *25*, 560–562; c) S. Kuwata, T. Nagano, A. Matsubayashi, Y. Ishii, M. Hidai, *Inorg. Chem*. **2002**, *41*, 4324–4330; d) A. Matsubayashi, S. Kuwata, Y. Ishii, M. Hidai, *Chem. Lett.* **2002**, 460–461; e) T. Nagano, S. Kuwata, Y. Ishii, M. Hidai, *Organometallics*, **2000**, *19*, 4176–4178.

[11] H. Kato, H. Seino, Y. Mizobe, M. Hidai, *Inorg. Chim. Acta* **2002**, *339*, 188–192.

[12] a) K. Iwasa, H. Seino, F. Niikura, Y. Mizobe, Dalton Trans. **2009**, 6134–6140; b) K. Iwasa, H. Seino, Y. Mizobe, *J. Organomet. Chem.* **2009**, *694*, 3775–3780; c) K. Arashiba, S. Matsukawa, Y. Tanabe, S. Kuwata, Y. Ishii, *Inorg. Chem. Commun.* **2008**, *11*, 587–590; d) K. Arashiba, Y. Tanabe, Y. Ishii, *Chem. Lett.* **2007**, *36*, 622–623; e) H. Kajitani, H. Seino, Y. Mizobe, *Organometallics*, **2007**, *26*, 3499–3508; f) T. Amitsuka, H. Seino, M. Hidai, Y. Mizobe, *Organometallics*, **2006**, *25*, 3034–3039; g) F. Takagi, H. Seino, Y. Mizobe, M. Hidai, *Organometallics*, **2002**, *21*, 694–699.

[13] a) M. A. F. Hernandez-Gruel, I. T. Dobrinovitch, F. J. Lahoz, L. A. Oro, J. J. Pérez-Torrente, *Organometallics* **2007**, *26*, 6437–6446; b) M. A. F. Hernandez-Gruel, F. J. Lahoz, I. T. Dobrinovich, F. J. Modrego, L. A. Oro, J. J. Pérez-Torrente, *Organometallics* **2007**, *26*, 2616–2622; c) M. A. Casado, J. J. Pérez-Torrente, M. A. Ciriano, I. T. Dobrinovitch, F. J. Lahoz, L. A. Oro, *Inorg. Chem.* **2003**, *42*, 3956–3964; d) M. A. F. Hernandez-Gruel, J. J. Pérez-Torrente, M. A. Ciriano, A. B. Rivas, F. J. Lahoz, I. T. Dobrinovitch, L. A. Oro, *Organometallics* **2003**, *22*, 1237–1249; e) M. A. F. Hernandez-Gruel, J. J. Pérez-Torrente, M. A. Ciriano, J. A. López, F. J. Lahoz, L. A.

Oro, *Eur. J. Inorg. Chem.* **1999**, 2047–2050; f) M. A. F. Hernandez-Gruel, J. J. Pérez-Torrente, M. A. Ciriano, F. J. Lahoz, L. A. Oro, *Angew. Chem. Int. Ed.* **1999**, *38*, 2769–2771; g) M. A. Casado, J. J. Pérez-Torrente, M. A. Ciriano, A. J. Edwards, F. J. Lahoz, L. A. Oro, *Organometallics* **1999**, *18*, 5299–5310.

[14] a) M. A. Casado, J. J. Pérez-Torrente, M. A. Ciriano, L. A. Oro, A. Orejón, C. Claver, *Organometallics* **1999**, *18*, 3035–3044; b) M. A. Casado, M. A. Ciriano, A. J. Edwards, F. J. Lahoz, L. A. Oro, J. J. Pérez-Torrente, *Organometallics* **1999**, *18*, 3025–3034; c) R. Atencio, M. A. Casado, M. A. Ciriano, F. J. Lahoz, J. J. Pérez-Torrente, A. Tiripicchio, L. A. Oro, *J. Organomet. Chem.* **1996**, *514*, 103–110.

[15] M. A. Casado, M. A. Ciriano, A. J. Edwards, F. J. Lahoz, J. J. Pérez-Torrente, L. A. Oro, *Organometallics* **1998**, *17*, 3414–3416.

[16] a) T. Amitsuka, H. Seino, M. Hidai, Y. Mizobe, *Organometallics* **2006**, *25*, 3034–3039; b) W.-Y. Yeh, H. Seino, T. Amitsuka, S. Ohba, M. Hidai, Y. Mizobe, *J. Organomet. Chem.* **2004**, *689*, 2338–2345; c) S. Nagao, H. Seino, M. Hidai, Y. Mizobe, *J. Organomet. Chem.* **2003**, *669*, 124–134; d) T. Kochi, Y. Nomura, Z. Tang, Y. Ishii, Y. Mizobe, M. Hidai, *J. Chem. Soc., Dalton Trans.* **1999**, 2575–2582; e) Z. Tang, Y. Nomura, S. Kuwata, Y. Ishii, Y. Mizobe, M. Hidai, *Inorg. Chem.* **1998**, *37*, 4909–4920.

[17] a) S. Kabashima, S. Kuwata, K. Ueno, M. Shiro, M. Hidai, *Angew. Chem. Int. Ed.* **2000**, *39*, 1128–1131; b) S. Kuwata, M. Andou, K. Hashizume, Y. Mizobe, M. Hidai, *Organometallics* **1998**, *17*, 3429–3436; c) Z. Tang, Y. Nomura, Y. Ishii, Y. Mizobe, M. Hidai, *Organometallics* **1997**, *16*, 151–154; d) K. Hashizume, Y. Mizobe, M. Hidai, *Organometallics* **1996**, *15*, 3303–3309.

[18] J. J. Pérez-Torrente, M. V. Jiménez, M. A. Hernández-Gruel, M. J. Fabra, F. J. Lahoz, L. A. Oro, *Chem. Eur. J.* **2009**, *15*, 12212–12222.

[19] a) A. M. Arif, J. G. Hefner, R. A. Jones, S. U. Koschmieder, *Polyhedron* **1988**, *7*, 561–572; b) T. A. Bright, R. A. Jones, S. U. Koschmieder, C. M. Nunn, *Inorg. Chem.* **1988**, *27*, 3819–3825.

[20] A. B. Rivas, J. M. Gascón, F. J. Lahoz, A. I. Balana, A. J. Pardey, L. A. Oro, J. J. Pérez-Torrente, *Inorg. Chem.* **2008**, *47*, 6090–6104.

[21] A. G. Orpen, *J. Chem. Soc., Dalton Trans.* **1980**, 2509-2516.

[22] a) T. Amaya, H. Sakane, T. Muneishi, T. Hirao, *Chem. Commun*. **2008**, 765–767; b) D. Carmichael, L. Ricard, N. Seeboth, J. M. Brown, T. D. W. Claridge, B. Odell, *Dalton Trans*. **2005**, 2173–2181; d) H. Egold, D. Schwarze, U. Flörke, *J. Chem. Soc., Dalton Trans*. **1998**, 1078–1084; e) F. P. Cossío, P. de la Cruz, A. de la Hoz, F. Langa, N. Martín, P. Prieto, L. Sánchez, *Eur. J. Org. Chem*. **2000**, 2407–2415; f) P. J. Heard, K. Kite, J. S. Nielsen, D. A. Tocher, *J. Chem. Soc., Dalton Trans*. **2000**, 1349–1356; g) J. Lu, D. Ma, J. Hu, W. Tang, D. Zhu, *J. Chem. Soc., Dalton Trans*. **1998**, 2267–2273; h) A. Gelling, M. D. Olsen, K. G. Orrell, A. G. Osborne, V. Šik, *Chem. Commun*. **1997**, 587–588; i) A. Gogoll, J. Örnebro, H. Greenberg, J. E. Bäckvall, *J. Am. Chem. Soc.* **1994**, *116*, 3631–3632.

[23] a) C. L. Perrin, T. J. Dwyer, *Chem. Rev.* **1990**, *90*, 935–967; b) E. W. Abel, T. P. J. Coston, K. G. Orrell, V. Šik, D. Stephenson, *J. Magn. Reson.* **1986**, *70*, 34–53; c) R. R. Ernst, G. Bodenhausen, A. Wokau, *Principles of Nuclear Magnetic Resonance in One and Two Dimensions*, Oxford University Press, Oxford, 1983.

[24] Cross peaks were integrated and processed with the EXSYCalc sofware distributed by Mestrelab research (http://www.mestrec.com).

[25] S. H. Gutowsky, C. H. Holm, *J. Chem. Phys*. **1956**, *25*, 1228–1234.

[26] L. R. Nevinger, J. B. Keister, *Organometallics* **1990**, *9*, 2312–2321, and references therein.

[27] K. A. Azam, S. E. Kabir, A. Miah, M. W. Day, K. I. Hardcastle, E. Rosenberg, A. J. Deeming, *J. Organomet. Chem.* **1992**, *435*, 157–167.

[28] A. Deeming, C. Forth, Md. I. Hyder, S. Kabir, E. Nordlander, F. Rodgers, B. Ullmann, *Eur. J. Inorg. Chem.* **2005**, 4352–4360.

[29] Md. I. Hyder, N. Begum, Md. D. H. Sikder, G. M. G. Hossain, G. Hogarth, S. E. Kabir, C. J. Richard, *J. Organomet. Chem.* **2009**, *694*, 304–308.

[30] A. Matsubayashi, S. Kuwata, Y. Ishii, M. Hidai, *Chem. Lett.* **2002**, 460–461.

[31] J. -F. Riehl, N. Koga, K. Morokuma, *J. Am. Chem. Soc.* **1994**, *116*, 5414–5424.

[32] a) R. Graves, J. M. Homan, G. L. Morgan, *Inorg. Chem.* **1970**, *9*, 1592–1593. b) V. Küllmer, H. Vahrenkamp, *Chem. Ber.* **1976**, *109*, 1560–1568.

[33] a) L. Han, L. -X. Shi, L. -Y. Zhang, Z. -N. Chen, M. -C. Hong, *Inorg. Chem. Commun.* **2003**, *6*, 281–283; b) J. R. Long, L. S. McCarty, R. H.Holm, *J. Am. Chem. Soc.* **1996**, *118*, 4603–4616; c) Y.-H. Qin, M.-M. Wu, Z.-N. Chen, *Acta Crystallogr., Sect. E: Struct. Rep. Online*, **2003**, *59*, m317; d) W. -N. Zhao, L. Han, C. -C. Luo, *Acta Crystallogr., Sect. C: Cryst. Struct. Commun.* **2008**, *64*, m280.

[34] a) P. Espinet, C. Hernández, J. M. Martín-Alvarez, J. A. Miguel, *Inorg. Chem.* **2004**, *43*, 843–845; b) M. V. Jiménez, J. Caballero, E. Sola, F. J. Lahoz, L. A. Oro, *Inorg. Chim. Acta* **2004**, *357*, 1948–1954; c) M. A. Ciriano, J. J. Pérez-Torrente, F. J. Lahoz, L. A. Oro, *J. Chem. Soc.; Dalton Trans.* **1992**, 1831–1837; d) G. Henkel, M. Kriege, K. Matsumoto, J. *Chem. Soc., Dalton Trans.* **1988**, 657–659.

[35] a) P. J. Alonso, O. Benedí, M. J. Fabra, F. J. Lahoz, L. A. Oro, J. J. Pérez-Torrente, *Inorg. Chem.* **2009**, *48*, 7984–7993. b) N. G. Connelly, G. Garcia, *J. Chem. Soc., Dalton Trans.* **1987**, 2737–2749.

[36] a) *Bonding Energetics in Organometallic Compounds*, T. J. Marks, Ed., ACS Symposium Series, Vol. 428, Washington, DC, 1990; b) X. -J. Qi, L. Liu, Y. Fu, Q. -X.

Guo, *Organometallics* **2006**, *25*, 5879–5886; c) D. Wang, R. J. Angelici, *J. Am. Chem. Soc.* **1996**, *118*, 935–942; d) Y. -M. Chen, P. B. Armentrout, *J. Am. Chem. Soc.* **1995**, *117*, 9291–9304; e) D. Dai, K. Balasubramanian, *New J. Chem.* **1991**, *15*, 721–726; f) J. A. Martinho-Simões, J. L. Beauchamp, *Chem. Rev.* **1990**, *90*, 629–6888.

[37] a) A. N. Startsev, *J. Mol. Catal. A: Chem.* **2000**, *152*, 1–13; b) A. N. Startsev, *Catal. Rev.-Sci. Eng.* **1995**, *37*, 353–423; c) B. Delmon, G. F. Froment, *Catal. Rev. Sci. Eng.* **1996**, *38*, 69–100.

[38] a) C. Bianchini, A. Meli, *Acc. Chem. Res.* **1998**, *31*, 109–116; b) M. D. Curtis, S. H. Druker, *J. Am. Chem. Soc.* **1997**, *119*, 1027–1036; c) C. Bianchini, A. Meli, *J. Chem. Soc., Dalton Trans.* **1996**, 801–814; d) R. A. Sánchez-Delgado, *J. Mol. Catal. A: Chem.* **1994**, *86*, 287–307.

[39] a) X. -D. Wen, T. Zeng, B. -T. Teng, F.- Q. Zhang, Y. –W. Li, J. Wang, H. Jiao, J. Mol. Catal. A: Chem. **2006**, *249*, 191–200; b) S. Cristol, J. F. Paul, E. Payen, D. Bougeard, S. Clémendot, F. Hutschka, *J. Phys. Chem. B*, **2002**, *106*, 5659–5667; c) V. Alexiev, R. Prins, Th. Weber, *Phys. Chem. Chem. Phys.* **2001**, *3*, 5326–5336. d) S. Cristol, J. F. Paul, E. Payen, D. Bougeard, S. Clémendot, F. Hutschka, *J. Phys. Chem. B* **2000**, *104*, 11220–11229

[40] a) M. Breysse, E. Furimsky, S. Kasztelan, M. Lacroix, G. Perot, *Catal. Rev.* **2002**, *44* 651–735; b) M. Lacroix, S. Yuan, M. Brysse, C. Dormieux-Morin, J. Fraissard, *J. Catal.* **1992**, *138*, 409–412.

[41] a) A. Scaffidi, L. Vivier, A. Travert, F. Maugé, S. Kasztelan, C. Scott, G. Pérot, *Stud. Surf. Sci. Catal.* **2001**, *138*, 31–38; b) E. J. M. Hensen, H. J. A. Brans, G. M. H. J. Lardinois, V. H. J. de Beer, J. A. R. van Veen, R. A. van Santen, *J. Catal.* **2000**, *192*, 98–107.

[42] a) M. Sun, A. E. Nelson, J. Adjaye, *J. Catal.* **2005**, *233*, 411–421; b) A. Travert, H. Nakamura, R. A. van Santen, S. Cristol, J. -F. Paul, E. Payen, *J. Am. Chem. Soc.* **2002**, *124*, 7084–7095.

[43] a) A. Ienco, M. J. Calhorda, J. Reinhold, F. Reineri,| C. Bianchini, M. Peruzzini, F. Vizza, C. Mealli, *J. Am. Chem. Soc.* **2004**, *126*, 11954–11965; b) T. B. Rauchfuss, *Inorg. Chem.* **2004**, *43*, 14–23; c) R. C. Linck, R. J. Pafford, T. B. Rauchfuss, *J. Am. Chem. Soc.* **2001**, *123*, 8856–8857; d) Z. K. Sweeney, J. L. Polse, R. A. Andersen, R. G. Bergman, *Organometallics* **1999**, *18*, 5502–5510; e) M. Rakowski DuBois, *Chem. Rev.* **1989**, *89*, 1–9; f) C. Bianchini, C. Mealli, A. Meli, M. Sabat, *Inorg. Chem.* **1986**, *25*, 4617–4618.

[44] G. Giordano, R. H. Crabtree, *Inorg. Synth.* **1979**, *19*, 218–220.

[45] E. W. Abel, M. A. Bennett, G. Wilkinson, *J. Chem. Soc.* **1959**, 3178–3182.

[46] D. E. Roe, A. G. Masey, *J. Organomet. Chem.* **1979**, *28*, 273–279.

[47] J. L. Herde, J. C. Lambert, C. V. Senoff, *Inorg. Synth.* **1974**, *15*, 18–20.

[48] F. Bonati, G. Wilkinson, *J. Chem. Soc.* **1964**, 3156–3160.

[49] S. R. Robinson, B. L. Shaw, *J. Chem. Soc.* **1965**, 4997–5001.

[50] R. Usón, L. A. Oro, J. Cabeza, *Inorg. Synth.* **1985**, *23*, 126–130.

[51] J. Jeener, B. H. Meier, P. Bachmann, R. R. Ernst, *J. Chem. Phys.* **1979**, *71*, 4546–4553.

[52] C. Perrin, *J. Magn. Resn.* **1989**, *82*, 619–621.

[53] M. J. Frisch, *et al*. Gaussian 03, revision E.01; Gaussian, Inc.: Wallingford, CT, 2004 (Complete citation in the Supporting information).

[54] SAINT: Area-Detector Integration Software.; Bruker AXS, Madison, **1995**.

[55] a) SADABS: Area Detector Absorption Correction; Bruker-AXS, Madison, **1996**; b) R. H. Blessing, *Acta Crystallogr. Sect A* **1995**, *51*, 33-38.

[56] SHELXS86: G.M. Sheldrick, *J. Mol. Struct.* **1985**, *130*, 9-16.

[57] M. C. Burla, M. Camalli, B. Carrozzini, G. L. Cascarano, G. Giacovazzo, G. Polidori, R. Spagna, *J. Appl. Cryst.* **2003**, *36*, 1103.

[58] SHELXL-97 Program for Crystal Structure Refinement, G. M. Sheldrick, University of Göttingen, Göttingen, **1997**.

Table 1. Selected bond distances (A) and angles for the hydrido trinuclear clusters [$Rh_3(\mu$-H)(μ_3-S)$_2${P(OPh)$_3$}$_4$(cod)] (**1**) and [$Rh_2Ir_2(\mu$-H)(μ_3-S)$_2${P(OPh)$_3$}$_4$(cod)] (**4**).

	1	**4**		**1**	**4**
Rh(1)-Rh(2)	2.9332(5)	3.0843(5)			
Rh(1)-Rh(3)/Ir	3.0774(5)	2.9480(4)	Rh(2)-Rh(3)/Ir	3.0839(5)	3.0298(4)
Rh(1)-S(1)	2.3505(11)	2.3502(11)	Rh(2)-S(1)	2.3533(10)	2.3463(11)
Rh(1)-S(2)	2.3501(11)	2.3481(11)	Rh(2)-S(2)	2.3502(12)	2.3406(12)
Rh(1)-P(1)	2.1939(11)	2.1835(11)	Rh(2)-P(3)	2.1944(12)	2.1824(12)
Rh(1)-P(2)	2.2072(12)	2.1993(11)	Rh(2)-P(4)	2.1968(11)	2.1866(12)
Rh(3)/Ir-S(1)	2.3194(11)	2.3296(10)	Rh(3)/Ir-S(2)	2.3188(11)	2.3270(10)
Rh(3)/Ir-C(1)	2.163(4)	2.171(4)	Rh(3)/Ir-C(5)	2.157(4)	2.166(4)
Rh(3)/Ir-C(2)	2.194(4)	2.191(4)	Rh(3)/Ir-C(6)	2.185(4)	2.186(4)
Rh(3)/Ir-M(1)$^{\#}$	2.064(5)	2.066(5)	Rh(3)/Ir-M(2)$^{\#}$	2.057(3)	2.061(3)
P(1)-O*	1.617(2)	1.620(2)	P(2)-O*	1.610(2)	1.609(2)
P(3)-O*	1.610(2)	1.612(2)	P(4)-O*	1.617(2)	1.614(2)
C(1)-C(2)	1.390(6)	1.398(6)	C(5)-C(6)	1.388(6)	1.399(6)
S(1)-Rh(1)-S(2)	82.60(4)	83.21(4)	S(1)-Rh(2)-S(2)	82.53(4)	83.46(4)
S(1)-Rh(1)-P(1)	94.63(4)	94.43(4)	S(1)-Rh(2)-P(3)	90.30(4)	90.22(4)
S(1)-Rh(1)-P(2)	172.62(4)	173.10(4)	S(1)-Rh(2)-P(4)	177.83(5)	177.68(4)
S(2)-Rh(1)-P(1)	177.22(4)	175.81(4)	S(2)-Rh(2)-P(3)	172.59(4)	173.68(4)
S(2)-Rh(1)-P(2)	90.24(4)	89.94(4)	S(2)-Rh(2)-P(4)	95.36(5)	94.64(4)
P(1)-Rh(1)-P(2)	92.53(4)	92.36(4)	P(3)-Rh(2)-P(4)	91.79(5)	91.67(5)

S(1)-Rh(3)/Ir-S(2)	83.96(4)	84.13(4)	M(1)-Rh(3)/Ir-M(2)[#]	86.57(14)	86.04(14)
S(1)-Rh(3)/Ir-M(1)[#]	175.45(12)	177.06(11)	S(2)-Rh(3)/Ir-M(1)[#]	95.24(10)	95.11(10)
S(1)-Rh(3)/Ir-M(2)[#]	94.61(11)	94.95(11)	S(2)-Rh(3)/Ir-M(2)[#]	174.88(10)	175.43(9)
Rh(1)-S(1)-Rh(2)	77.16(3)	82.10(3)	Rh(1)-S(2)-Rh(2)	77.23(3)	82.27(3)
Rh(1)-S(1)-Rh(3)/Ir	82.44(3)	78.09(3)	Rh(1)-S(2)-Rh(3)/Ir	82.46(3)	78.18(3)
Rh(2)-S(1)-Rh(3)/Ir	82.59(3)	80.78(3)	Rh(2)-S(2)-Rh(3)/Ir	82.67(4)	80.95(3)
P(1)-O-C[*]	123.7(2)	123.7(2)	P(3)-O-C[*]	129.1(2)	128.0(2)
P(2)-O-C[*]	128.1(3)	128.2(3)	P(4)-O-C[*]	124.7(2)	124.4(2)
C(2)-C(1)-C(8)	125.3(4)	124.7(4)	C(4)-C(5)-C(6)	125.7(4)	126.9(4)
C(1)-C(2)-C(3)	124.4(5)	123.3(5)	C(5)-C(6)-C(7)	123.9(5)	122.6(5)

[#] M(1) and M(2) represent the midpoints of the coordinated olefinic bonds, C(1)-C(2) and C(5)-C(6). [*] Mean values calculated for analogous bonds and angles in each phosphite moiety.

Table 2. ^{1}H 2D EXSY-derived rate constants (k_1 and k_{-1}/s^{-1}) and activation energies ($\Delta G_1^{\#}$ and $\Delta G_{-1}^{\#}$/kJ mol^{-1}) for the equilibrium **a** ⇆ **b** in trinuclear hydrido-sulfido clusters.[a]

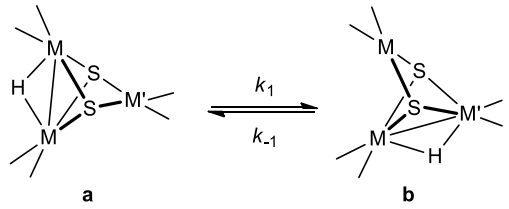

a **b**

Cluster	t_m (ms)	T_1 (ms)	k_1 (s^{-1}) [b]	k_{-1} (s^{-1}) [b]	$\Delta G_1^{\#}$ [c] (kJ mol^{-1})	$\Delta G_{-1}^{\#}$ [c] (kJ mol^{-1})	K = k_1/ k_{-1}
1	300	750	3.47	2.11	70.4	71.6	1.64
2	300	900	5.52	5.28	69.2	69.3	1.05
3	200	750	2.94	3.06	70.8	70.7	0.96
5	100	440	4.61	9.68	69.7	67.8	0.48
8	300	800	4.30	2.15	69.8	71.6	2.00

[a] 2D-EXSY spectra (500 MHz) were recorded at 300 K using saturated C_6D_6 solution of the clusters. [b] The integrations for the exchange cross-peak were processed using the EXSYCalc program to obtain the rate constants k_1 and k_{-1}. [c] Eyring equation was used to calculate activation energies $\Delta G_1^{\#}$ and $\Delta G_{-1}^{\#}$; $\Delta G^{\#} = -RT\ln(hk/k_BT)$; T is temperature in Kelvin, k_B is the Boltzmann's constant, and h is Planck's constant.

Figure and Scheme legends

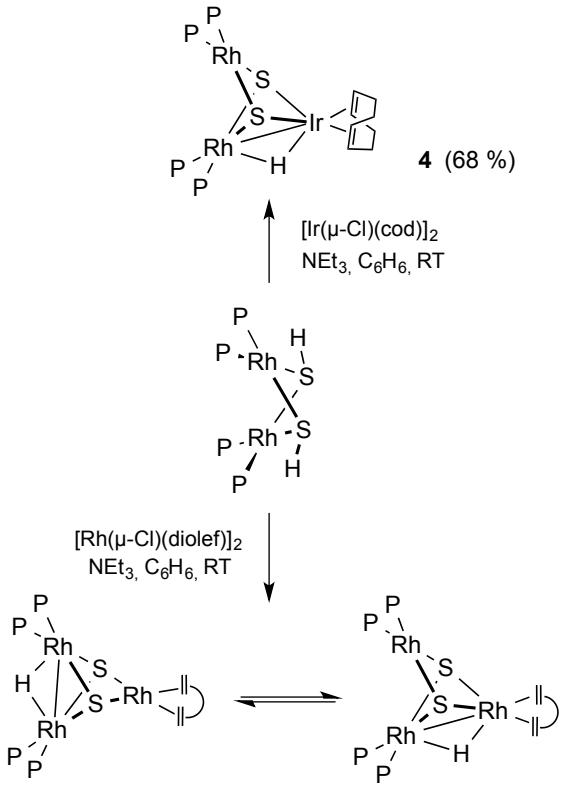

P = $P(OPh)_3$ **1** (diolef = cod, 82 %)
2 (diolef = nbd, 70 %)
3 (diolef = tfb, 56 %)

Scheme 1. Synthesis of trinuclear hydrido-sulfido clusters from $[Rh(\mu\text{-}SH)\{P(OPh)_3\}_2]_2$.

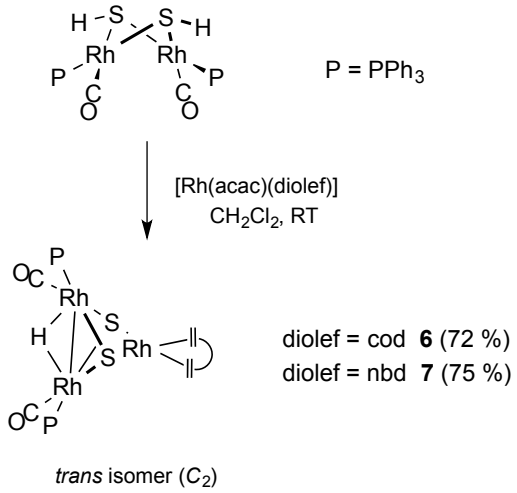

Scheme 2. Synthesis of trinuclear hydrido-sulfido clusters from $[Rh(\mu\text{-}SH)(CO)(PPh_3)]_2$.

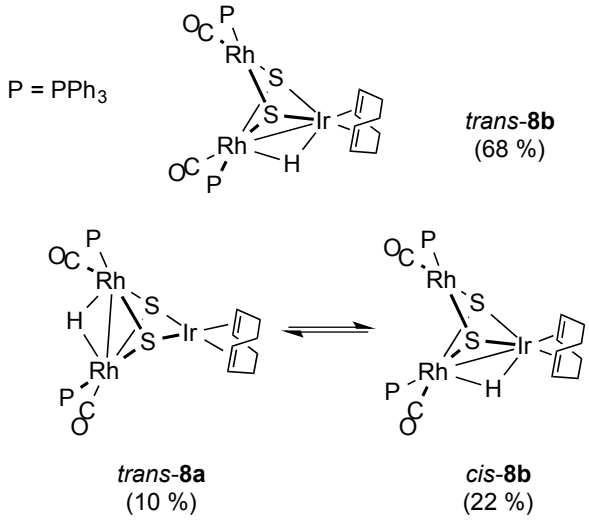

Scheme 3. Hydride exchange in the observed isomers of cluster **8**.

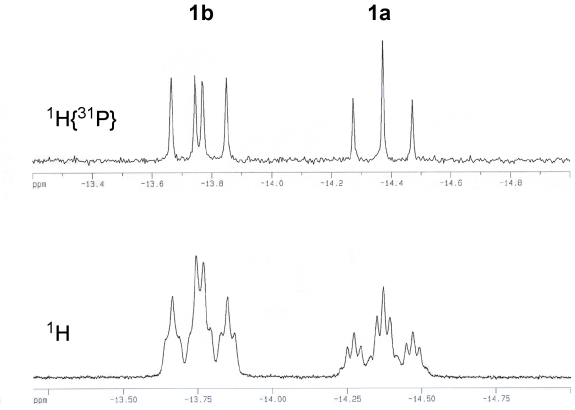

Figure 1. ^1H and $^1H\{^{31}P\}$ NMR spectra of **1** (hydride region) in C_6D_6 at 298 K.

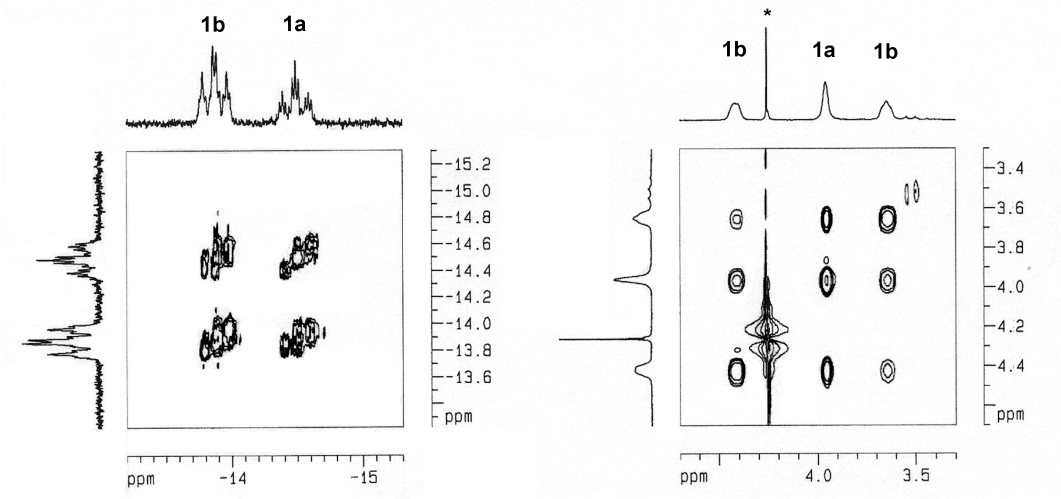

Figure 2. Selected regions of the $^{1}H–^{1}H$ NOESY NMR spectrum of **1** in C_6D_6 at 298 K: a) hydride region, b) olefinic =CH region (* CH_2Cl_2).

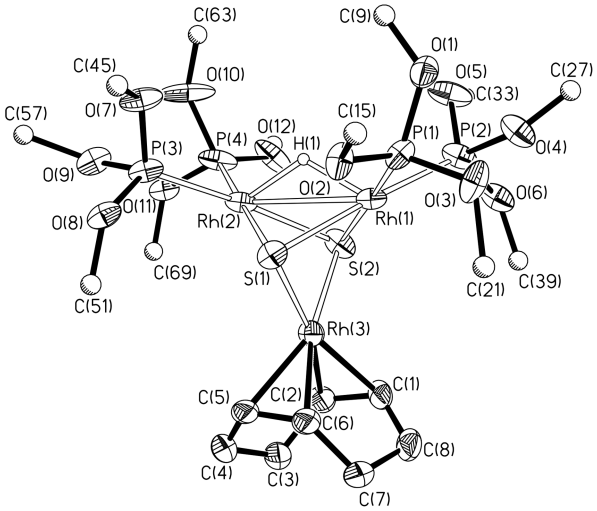

Figure 3. Molecular structure of cluster $[Rh_3(\mu\text{-}H)(\mu_3\text{-}S)_2\{P(OPh)_3\}_4(cod)]$ (**1**). Only *ipso* carbons of the phenyl rings have been represented for clarity.

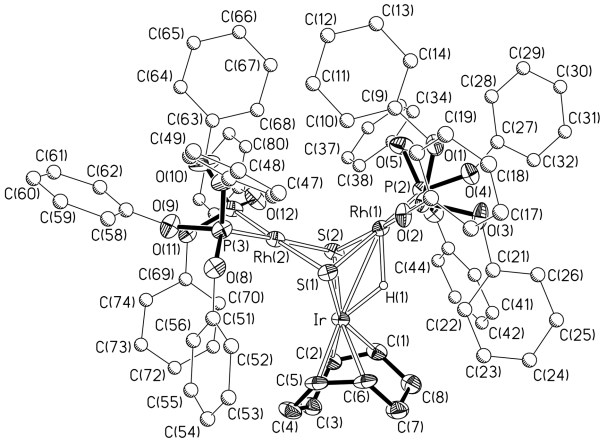

Figure 4. Molecular structure of cluster $[Rh_2Ir(\mu\text{-}H)(\mu_3\text{-}S)_2\{P(OPh)_3\}_4(cod)]$ (**4**). For clarity a simple ball and stick model has been used for the phenyl rings.

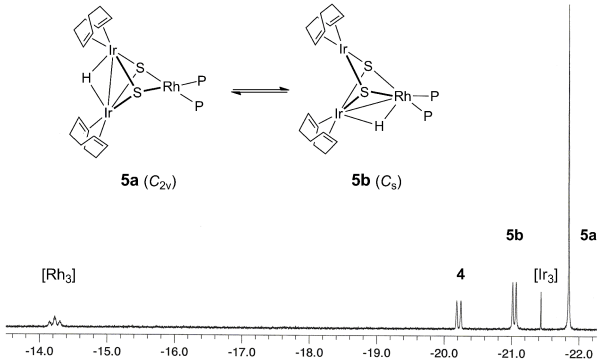

Figure 5. Hydride region of the ^1H NMR spectrum of the reaction of $[Rh(\mu\text{-}SH)\{P(OPh)_3\}_2]_2$ with $[Ir(\mu\text{-}OMe)(cod)]_2$ (1:1 molar ratio) in $[D_8]$-toluene at 298 K. $[Rh_3]$ = $[Rh_3(\mu\text{-}H)(\mu_3\text{-}S)_2\{P(OPh)_3\}_6]$, $[Ir_3]$ = $[M_3(\mu\text{-}H)(\mu_3\text{-}S)_2(cod)_3]$.

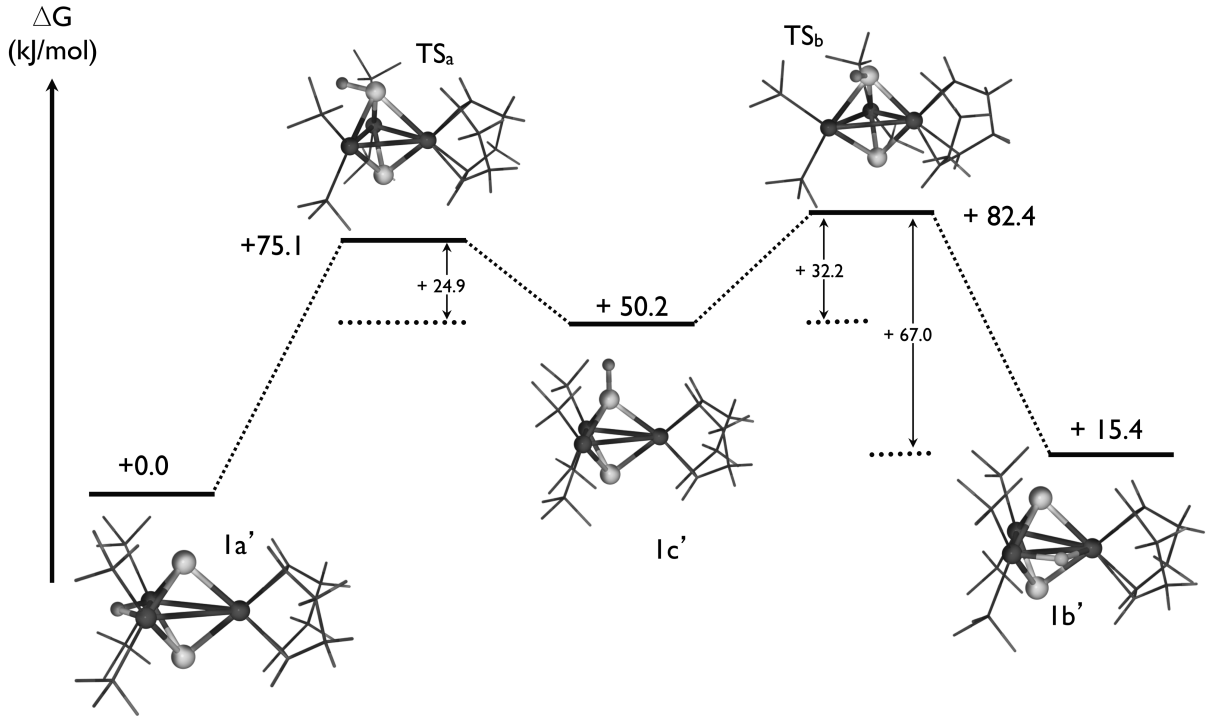

Figure 6. Relative free energies (ΔG, kJ mol^{-1}) in the gas phase and geometries along the pathway for the hydrogen migration in cluster model $[Rh_3(\mu\text{-}H)(\mu_3\text{-}S)_2(PH_3)_4(cod)]$.

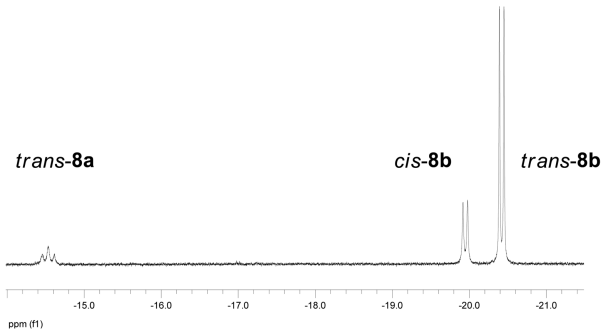

Figure 7. Hydride region of the ^{1}H NMR spectrum of cluster $[Rh_2Ir(\mu\text{-}H)(\mu_3\text{-}S)_2(CO)_2(PPh_3)_2(cod)]$ (**8**) in C_6D_6 at 298 K.

Text for the Table of Contents

Sulfido clusters:

Dynamic hydrido-sulfido clusters: Trinuclear clusters with the core $[M_3(\mu\text{-}H)(\mu_3\text{-}S)_2]$ have been prepared from bis-(hydrosulfido)-bridged dinuclear rhodium(I) compounds. The migration of the hydride ligand between the edges of the metallic triangle through a mechanism assisted by the sulfido ligands has been observed in some cases. The movement of the hydride ligand in the clusters can be described as a proton migrating over the electronic density at the rhodium centers the sulfido ligand.

M. V. Jiménez, F. J. Lahoz, L. Lukešová, J. R. Miranda, F. J. Modrego, D. H. Nguyen, L. A. Oro, J. J. Pérez-Torrente**……..…… Page – Page

Hydride Mobility in Trinuclear Sulfido Clusters with the Core $[Rh_3(\mu\text{-}H)(\mu_3\text{-}S)_2]$: Molecular Models for Hydrogen Migration on Metal Sulfide Hydrotreating Catalysts

Keywords: cluster compounds • rhodium • sulfur • hydrides